Elsevier Editorial System(tm) for Computers in Biology and Medicine

Manuscript Draft

Manuscript Number: CBM-D-15-00639R1

Title: Biomechanical Implications of Excessive Endograft Protrusion into the Aortic Arch after Thoracic Endovascular Repair

Article Type: Full Length Article

Keywords: thoracic endovascular aortic repair (TEVAR), bird-beak, stent-graft, endograft collapse/infolding; fluid-structure interaction

Corresponding Author: Dr. Salvatore Pasta, Ph.D.

Corresponding Author's Institution: Fondazione RiMED

First Author: Antonino Rinaudo

Order of Authors: Antonino Rinaudo; Giuseppe M Raffa; Francesco Scardulla; Michele Pilato; Cesare Scardulla; Salvatore Pasta, Ph.D.

Abstract: Endografts placed in the aorta for thoracic endovascular aortic repair (TEVAR) may determine malappositioning to the lesser curvature of the aortic wall, thus resulting in a devastating complication known as endograft collapse. This premature device failure commonly occurs in young individuals after TEVAR for traumatic aortic injuries as a result of applications outside the physical conditions for which the endograft was designed. In this study, an experimentally-calibrated fluid-structure interaction (FSI) model was developed to assess the hemodynamic and stress/strain distributions acting on the excessive protrusion extension (PE) of endografts deployed in four young patients underwent TEVAR. Endograft infolding was experimentally measured for different hemodynamic scenarios by perfusion testing and then used to numerically calibrate the mechanical behavior of endograft PE. Results evinced that the extent of endograft can severely alter the hemodynamic and structural loads exerted on the endograft PE. Specifically, PE determined a physiological aortic coarctation into the aortic arch characterized by a helical flow in the distal descending aorta. High device displacement and transmural pressure across the stent-graft wall were found for a PE longer than 21 mm. Finally, marked intramural stress and principal strain distributions on the protruded segment of the endograft wall may suggest failure due to material fatigue. These critical parameters may contribute to the endograft collapse observed clinically and can be used to design new devices more suitable for young individuals to be treated with an endoprosthesis for TEVAR of blunt traumatic aortic injuries.

Conflict of Interest Statement

Fondazione
Ri.MED

Salvatore Pasta, PhD
Fondazione RiMED,
Via Bandiera, 11
90133 Palermo
Tel: +39 091 3815681
Fax:+39 091 3815682
email:sap62@pitt.edu

Dear Editor,

With the present, Salvatore Pasta as corresponding author of the manuscript titled: “Biomechanical Implications of Excessive Endograft Protrusion into the Aortic Arch after Thoracic Endovascular Repair” submitted for publication to Computers in Biology and Medicine on 24-July-2015 states that:

- All authors do not have to disclose any financial or personal relationships with other people or organizations that could inappropriately influence (bias) their work.

Such statement can be confirmed by members of Fondazione RiMED, University of Pittsburgh and ISMETT.

Should you have any questions, please contact our office at +39 091 6657170 or email sap62@pitt.edu

Best Regards,

Salvatore Pasta, PhD,
Professor of Mechanical Engineering,
Fondazione RiMED,
Via Bandiera n.11,
90133, Palermo, Italy,
Tel. office: +39 091 6657170
fax: +39 091 484334
mobile: +39 334 9379694
email: sap62@pitt.edu

Reviewer #1

We thank the reviewer for his or her valuable comments. We have taken these comments into careful consideration when preparing the revised manuscript and feel that the critiques led directly to an improved submission. We hope that the reviewer agrees. All changes made to the document were highlighted in yellow.

Comment: The last sentence is not accurate. The referenced studies are not only on post traumatic injuries and Bandorski'spaper include only 16 TEVAR for various pathologies which is very poor. A review published by Jonker FH et al. should be cited (J EndovascTher. 2010 Dec;17(6):725-34), as well as ref 6 which report 0.4% of infolding.

Reply: Indeed, the incidence of endograft collapse is difficult so that the reported ranges were deleted. The reference to Jonker and the incidence reported in reference n.6 were reported with the following text: "The incidence rates of endograft collapse after TEVAR for traumatic injuries are not well defined [8, 11], although collapses usually present in the early post-operative period (median time of 15 days) [12]. It has been recently reported that the Gore TAG thoracic endoprosthesis (W. L. Gore and Assoc, Flagstaff, Ariz) accumulated a 0.4% frequency rate of device collapse among 33,000 endografts distributed worldwide [6]. However, collapse rates likely differ for other available endografts. "

Comment: Second paragraph : J EndovascTher. 2010 Dec;17(6):725-34: this review should be included to elucidate the mechanism involved. The last sentence is really difficult to understand and should be explain in another way.

Reply: The reference to Jonker's review was added. The last sentence was rewritten with the following:"However, the bird-beak configuration is not the only determinant of stent-graft collapse, because this phenomenon has not been observed with high frequency in patients with thoracic aneurysms (10.1% of 139 TAG collapses), many of whom can present a proximal bird-beaking in the aortic arch [6]."

Comment: The sentence : "Low systolic pressure was observed into LSA for the patient with coverage of left subclavian, suggesting malperfusion of distal organs" should be removed. In real life condition, LSA coverage is mostly asymptomatic, as the perfusion of the left arm is performed by the vertebral artery and others collaterals.

Reply: This sentence was deleted.

Comment: The first sentence should be rephrasing, as the authors didn't include in their work several oversizing or arch configuration. It should also be discussed the involvement of the aortic arch anatomy of the patient, which seems to be a bovine arch.

Reply: The sentence was rephrased with the following:"These factors may lead to an increased risk of endograft collapse for those young patients undergoing TEVAR for traumatic aortic injuries."

The impact of bovine arch was discussed with the following sentence located in the last paragraph of the Discussion Section:"In this study, the phantom model was obtained from a patient with a bovine arch, and this can impact the measurement of the flow-induced endograft displacement used to initially calibrate the computational model."

Comment: The authors should further extent the impact of their findings on the new design for thoracic endograft in young patients.

Reply: As stated in the conclusion, the proposed approach can be used to design new devices as well as to test the new Comfortable Gore TAG device. We also recognize that these findings are confined to the investigated endograft and aortic geometries. Therefore, this study will be extended in the future to the new Comfortable Gore TAG device. Nothing has been added to the text, if permitted.

Reviewer #2

We thank the reviewer for his or her valuable comments. We have taken these comments into careful consideration when preparing the revised manuscript and feel that the critiques led directly to an improved submission. We hope that the reviewer agrees. All changes made to the document were highlighted in yellow.

Comment: In this study, the aortic phantom was made of silicon. Silicon has material properties that are very different than that of blood vessels. How do the authors justify using silicon in place of blood vessel tissue? The experimental portion of the study could very much benefit from using natural tissue rather than a silicon phantom. I understand that the geometry would not be patient-specific anymore in case of using cadaveric tissue, but the realistic mechanical behavior of vessel tissue could very well be advantageous for this study.

Reply:As suggested in many clinical studies (see reference 6,8, 10-13), endograft collapse is mainly caused by a tight aortic arch so that the particular anatomy of the patient plays a key role. Therefore, a patient-specific anatomy is highly recommendable. Most importantly, it will be very hard, or even impossible, to find a cadaveric tissue with an aortic arch diameter that permits to guarantee the endograft oversizing realized in the clinical setting. In this patient, surgeons decided for a device oversizing of 11%, according the instruction of use (IFU) for the Gore TAG stent-graft. This oversizing is essential for adequate fixation at the level of the proximal landing zone and is considered a major risk factor for collapse (see reference). Additionally, cadaveric tissues are usually collected from cadavers of adults, with aortic stiffness higher than that of young individuals. So, even a cadaveric tissue does not represent the real clinical scenario.We retained to give high priority to the patient-specific aortic-anatomy and device-oversizing rather than the mechanical behavior of the aorta.

With concern to silicone, experimental tensile testing evinced that Young modulus of silicone is comparable (or slightly more elastic)than that of the aorta (see unpublished data of Schlicht at http://deepblue.lib.umich.edu/handle/2027.42/84613).Additionally, several studies in literature adopted

silicone phantom to mimic the aorta and study aortic-related diseases (Tsai, J VascSurg, 2008 and Rudenick, J Vas Surg, 2013).

We recognize that this is a limit of our investigation so that this was clarified at the end of Discussion Section with the following sentences:"The compliance of the silicone phantom model may differ from those occurring in the actual young aorta of the investigated patient case. The distensibility of silicone phantom allows mimicking that of a human aorta as this elastic material was used in several in-vitro models to study aortic diseases [16, 31]. However, the utilize of a patient-specific silicone phantom allowed us to study the actual aortic arch anatomy and device oversizing, which are the main contributors to endograft collapse [8, 10]."

Comment: Modeling the aorta as an isotropic tissue is too simplistic. Anisotropic material properties of aorta are readily available and the material model is also available in the FE software of choice here, Abaqus. I recommend that authors repeat the simulations by using an anisotropic material model for aorta.

Reply: We do recognize that an anisotropic constitutive formulation will better represent the aortic material properties. Please consider that patients here investigated were young individuals. Specifically, the preliminary FSI analysis was performed for a patient with age of 21 at the time of TEVAR (see Case 2 of Go et al. J VascSurg, 2008). Thus, the aorta of these patients is more elastic while most of anisotropic material properties are often derived from aortic tissues harvested by adults, which likely show increased aortic stiffness due to ageing. It should be also considered the effect of endograft on the aortic wall that constrains the motion of the aorta over the cardiac cycle so that the aortic compliance is mostly driven by the stiffer endograft.

The proposed hyperelastic, isotropic constitutive formulation was widely adopted by many FE analyses to study aortic diseases such ascending thoracic aortic aneurysm (Pasta et al, J Biomech, 2013), descending aortic aneurysm (Shang et al, Circulation, 2013) and abdominal aortic aneurysm (VandeGeest et al. Ann BiomEng, 2006). Most importantly,we demonstrated using different endograft

devices and artificial aortic arch angulations that the mechanism of endograft collapseis mostly driven by flow dynamics (Pasta et al, J EndovascTher, in press).

We prefer not to repeat all simulations, if the reviewer agrees. It is retained that the mechanical behavior of the aorta is well represented, although with limitations. The following sentence was therefore included at the end of Discussion Section to clarify the limit of our FSI analyses:"In the FSI analyses, an anisotropic constitutive formulation should better represent the real mechanical behavior of the aorta."

Comment: Why did the authors chose to do a one-way FSI analysis rather than two-way analysis? Also why the authors did not perform the whole FSI analysis in software Ansys which has the FSI capability? Transferring the results from Fluent to Abaqus does not seem intuitive to me.

Reply: We have tried to run two-way FSI analyses but faced with several numerical issues. The major difficult is inherent to the highly dynamic mechanics of endograft collapse. Due to the considerable endograft displacement into the aortic arch, the elements of fluid domains were highly distorted when the structural solution returned back to the flow solver. In our approach, the analytical formulation of each of Abaqus and Fluent software are solved independently. Unless a fully coupled solver with implicit formulation is used, we retain that it is very difficult to perform a two-way FSI analysis. MpCCI is commercial software specifically developed to couple FE solvers with a relatively easy approach (www.scapos.com). In this software, the solution exchange is performed similar to AnsysWorkbench by using a surface to exchange the flow solution with the structural solver. In our opinion, there is no reason to believe that this approach has altered the solution and results here presented.

Comment: Was turbulence in blood flow modeled here? If yes please explain how. If no please explain why you ignored turbulence.

Reply: The blood flow is usually assumed to be laminar in large vessels due to the low mean flow velocity (Morris et al., J Biomech 2004). Although the flow has lost its typical laminar characteristics after the endograft, the peak systolic flow in the descending aorta is low as shown by Figure 3. For the Case D with the highest peak systolic velocity, the flow in the descending aorta leads to a Reynolds number of 1710, which is lower than the threshold for transient flow (ie, 2300). Therefore, the laminar assumption is satisfied. The following text was added in the Methods Section:" This is a valid assumption since low mean flow velocities usually occur in large vessels [19]. Indeed, we found a Reynolds number of 1710 just distal to the endograft PE for the Case D with the highest peak-systolic flow velocity."

Comment: The authors claim that the FSI study presented here is experimentally validated. I did not see any comparison of experimental data to simulations results that demonstrate this validation. Please clarify how the validation was performed.

Reply: We agree with the reviewer comment that the term "experimentally-validated" was misinterpreted. The term "experimentally-validated" was replaced with the term "experimentally-calibrated" FSI model.

Minor Comments: Abstract suffers from several grammatical errors and is not written in proper English. Consider rewriting the abstract as some of the sentences are very hard to understand. For example: "Results evinced … endograft wall." This sentence is too long and hard to read."

Reply: fixed. The whole manuscript was polished by grammatical errors.

Minor Comment: As another example: This sentence is incorrect "This premature … designed." I think the authors meant " as a result of applications…"

Reply: fixed. The whole manuscript was polished by grammatical errors.

Minor Comment: Page 12, first paragraph: "Similarly, Cheng et al. [23] demonstrated that .. diameter." This sentence is incomplete.

Reply: fixed with the following: “Similarly, Cheng et al. [24] demonstrated that the lifting force depends on the graft diameter as well as the initial deployment position relative to the aortic arch of patients with TEVAR for aortic dissection.”

Reviewer #3

We thank the reviewer for his or her valuable comments. We have taken these comments into careful consideration when preparing the revised manuscript and feel that the critiques led directly to an improved submission. We hope that the reviewer agrees. All changes made to the document were highlighted in yellow.

Comment: In my opinion, the last part of the introduction ("Initially....discussed") should be placed in the methods.

Reply: If the reviewer agrees, we prefer not to place this part in the Methods since the same concept is in part repeated in the methodology.

Comment: What are the company details of "Metal Professional Company".

Reply: Details were added in the text.

Comment: - "For the aorta to deform in a physiological manner, the distal ends of supra-aortic vessels, aortic valve and descending aorta were fixed in all directions." - That is not physiological as we know that the aorta distends significantly both longitudinal and radial, and that the thoracic aorta displaces considerably, especially in a young patient [Rengier 2012 EJR]. I understand why you would like to fix it, but it is not correct to call that physiological...

Reply: The text “For the aorta to deform in a physiological manner” was deleted from the sentence.

Comment: - "Calibration of the bird-beak mechanical parameter under different hemodynamic conditions and bird-beak configurations revealed that the endograft stiffness increases with higher systemic pressure and flow rate (Figure 2). Moreover, the stiffness linearly increases as the PE decreases for a given hemodynamic condition. It is should be noted that the stiffness here reported does not represent the Young's modulus of endograft but rather the global endograft mechanical behavior

under a particular condition of flow-induced loads (i.e, pressure exerted on both the undersurface and the luminal surface of the protruded endograft wall), geometrical configuration (i.e., combination of PE and q), and device characteristics (i.e, geometry of nitinol frame)." - Stiffness does not seem the right term in this case. It is confusing for the reader as stiffness is usually considered mechanical stiffness by Young's modulus. A more dynamic term as endograft compliance/pulsatility seems more correct.

Reply: We fully agree with reviewer suggestion that the term "stiffness" was not properly used. Therefore, the "stiffness" term was replaced with the term "compliance" throughout the text.

Comment: - "Peak systolic pressure was found lower distal to the bird-beak configuration and markedly higher proximal to the ascending aorta and supra-aortic vessels." - A control image without a stent graft is missing here in figure 3.

Reply: Please look at Fig. 3 of our previously published study (Pasta et al J Vasc Surg,2013;57(5)1353-61) to observe the hemodynamic environment without the stent-graft. Indeed, the flow is quite laminar without the stent-graft so that the pressure was homogenous with a value of 114 mmHg in the aortic arch where the stent-graft was deployed for TEVAR. Reference to the article has been added to this sentence.

Comment: - "Additionally, the patient case with the longer PE exhibited higher pressure drop than that of the patient with a short birdbeak configuration (compare Case D with Case A)". - to me it seems that Case D actually has higher pressures in the aorta distal to the bird-beak than case A. Therefore the pressure drop in the descending aorta seems to be higher for Case A, with a short PE.

Reply: Indeed, the reviewer is right so that the sentence was deleted.

Comment: Table 2 misses p-values.

Reply: No statistical comparison was performed. Table 2 reported the computationally-predicted values of endograft parameters for each patient.

Comment: Why were drag forces on the endografts not calculated? It may shed light into this issue.

Reply: Although the drag force was not calculated, we retain that the transmural pressure gradient across the stent-graft wall is a similar parameter to quantify the risk of collapse. Indeed, we previously showed that the transmural pressure increase as the protruded stent-graft wall increases (see Pasta et al J Vasc Surg,2013;57(5)1353-61). This relationship is similar to the link between the drag force and the blood pressure reported by Fung and collaborators (reference n.24) in a previous issue of this journal. Therefore, the drag force is somewhat proportional to the trasmural pressure here reported. Nothing was added in the text if the reviewer agrees.

Comment: In the conclusion: A stronger message would strengthen the paper here. For instance, a rate of PE that increased changes of displacement significantly. It seems that protruding the endograft with more than 21 mm (case B), causes a very increased risk of displacement.

Reply: We thank reviewer suggestion. The following sentence was added in the conclusion to strength the message:“Indeed, a proximal bird-beaking with a PE longer than 21 mm may lead to a considerable endograft displacement into the aortic arch, and this may warrant clinical surveillance during follow-up.”

Biomechanical Implications of Excessive Endograft Protrusion into the Aortic Arch after Thoracic Endovascular Repair

Antonino Rinaudo[1], Giuseppe Maria Raffa[2], Francesco Scardulla[1], Michele Pilato[2], Cesare Scardulla[2], Salvatore Pasta[2,3]

[1] DICGIM, Universitá di Palermo, Palermo, Italy

[2] Department for the Treatment and Study of Cardiothoracic Diseases and Cardiothoracic Transplantation, Mediterranean Institute for Transplantation and Advanced Specialized Therapies (ISMETT), Palermo, Italy

[3] Fondazione Ri.MED, Palermo, Italy

Conflict of Interest: none

Sources of Financial Support: RiMED Foundation

Corresponding author:

Salvatore Pasta, PhD

NSQ Professor in Mechanical Engineering

Fondazione Ri.MED

Cell: +39 3349379694

Phone: +39 091 6041 111

FAX: +39 091 6041 122

e-mail: spasta@fondazionerimed.com

ABSTRACT

Endografts placed in the aorta for thoracic endovascular aortic repair (TEVAR) may determine malappositioning to the lesser curvature of the aortic wall, thus resulting in a devastating complication known as endograft collapse. This premature device failure commonly occurs in young individuals after TEVAR for traumatic aortic injuries as a result of applications outside the physical conditions for which the endograft was designed. In this study, an experimentally-calibrated fluid-structure interaction (FSI) model was developed to assess the hemodynamic and stress/strain distributions acting on the excessive protrusion extension (PE) of endografts deployed in four young patients underwent TEVAR. Endograft infolding was experimentally measured for different hemodynamic scenarios by perfusion testing and then used to numerically calibrate the mechanical behavior of endograft PE. Results evinced that the extent of endograft can severely alter the hemodynamic and structural loads exerted on the endograft PE. Specifically, PE determined a physiological aortic coarctation into the aortic arch characterized by a helical flow in the distal descending aorta. High device displacement and transmural pressure across the stent-graft wall were found for a PE longer than 21 mm. Finally, marked intramural stress and principal strain distributions on the protruded segment of the endograft wall may suggest failure due to material fatigue. These critical parameters may contribute to the endograft collapse observed clinically and can be used to design new devices more suitable for young individuals to be treated with an endoprosthesis for TEVAR of blunt traumatic aortic injuries.

Key words: thoracic endovascular aortic repair (TEVAR), bird-beak, stent-graft, endograft collapse/infolding; fluid-structure interaction

INTRODUCTION

Thoracic endovascular aortic repair (TEVAR) has emerged over the last decade as the preferential minimally invasive therapeutic modality for a variety of thoracic aortic pathologies, including traumatic thoracic aortic injuries [1-3]. TEVAR for traumatic injuries is effective but its outcome remains a concern especially in young patients [4, 5]. In these individuals, the endograft is often implanted "off-label", and device oversizing is essential for fixation at the level of the proximal landing zone [6]. This may ultimately induce to premature device failure and endograft collapse/infolding, which usually requires a secondary intervention by means of re-do TEVAR or conversion to open surgery with attendant high morbidity and mortality [7-10]. The incidence rates of endograft collapse after TEVAR for traumatic injuries are not well defined [8, 11], although collapses usually present in the early post-operative period (median time of 15 days) [12]. It has been recently reported that the Gore TAG thoracic endoprosthesis (W. L. Gore and Assoc, Flagstaff, Ariz) accumulated a 0.4% frequency rate of device collapse among 33,000 endografts distributed worldwide [6]. However, collapse rates likely differ for other available endografts.

A number of anatomic- and device-related factors may contribute to endograft infolding including a young healthy aorta with tight aortic arch and marked pulsatility, excessive stent-graft oversizing and material fatigue [8, 12, 13]. Endograft infolding–related mortality rates of 16.9% for asymptomatic patients and 27.3% for symptomatic patients within 3 years of diagnosis [11, 13, 14]. Collapses are most often observed when the proximal extent of the endograft is in the transverse arch with malapposition of the endograft wall along the lesser curvature of the aorta (the so-called "bird-beak" phenomenon) [9-11, 14]. Bird-beaking is not desirable because it

exposes the graft undersurface to the force of the bloodstream. However, the bird-beak configuration is not the only determinant of stent-graft collapse, because this phenomenon has not been observed with high frequency in patients with thoracic aneurysms (10.1% of 139 TAG collapses), many of whom can present a proximal bird-beaking in the aortic arch [6].

Although the bird-beak effect is often observed after TEVAR of traumatic injuries in young patients [11], collapses do not occur in all of them. It would be also desirable if these individuals with increased risk for developing such a complication would benefit of ad-hoc endografts to tailor their tight and elastic aortic arch. However, the mechanics of endograft collapse has not been clearly defined yet. The understanding of the mechanisms underlying endograft collapse may lead to the design of new devices for TEVAR in young patients. Therefore, we developed an experimentally-calibrated computational model to study the hemodynamic, wall stress and strain acting on the bird-beak configuration observed in four patients underwent TEVAR. Initially, endograft infolding was measured for different perfusion conditions and bird-beak configurations in a patient-specific phantom model. Then, infolding measurements were used as input for a fluid-structure interaction (FSI) model to tune the endograft mechanical property and then the displacement of the proximal protruded wall of the endograft. Finally, computational simulations were performed to estimate the intramural wall stress and principal strain distributions on the bird-beaking of four young patients underwent TEVAR for traumatic thoracic aortic injuries. The possible causes of endograft collapse are discussed.

METHODS

The role of hemodynamic loads on the infolding resulting from the bird-beak configuration of a thoracic endograft was explored using a case of a male patient who underwent TEVAR for a traumatic aortic injury, and subsequently developed stent-graft collapse with neurologic complications, as previously investigated by our group [14]. Once a phantom model of the patient aortic anatomy was obtained, the infolding resulting from the endograft deployment was assessed by perfusion testing and then used to calibrate the global mechanical behavior of the endograft implanted in this patient. Finally, the hemodynamic and the strain/stress distributions on the protruded stent-graft wall were predicted for four young patients with mean age of 32±9 yrs.

Phantom and Flow Circuit

To reconstruct the aortic geometry after TEVAR, the post-operative patient's CT scan was segmented using the vascular modeling toolkit VMTK as previously described [15]. Thus, the reconstructed patient-specific aortic geometry was transferred to the Metal Professional (River Road, WI, USA) in order to manufacture a compliant and transparent silicone phantom model. The latter represents a scale 1:1 of the patient's aortic anatomy after endovascular repair. Under no perfusion conditions, scissor-handle forceps were utilized to deploy a 26 mm x 10 cm Gore TAG thoracic endoprosthesis (TAG v1.5, W. L. Gore and Assoc, Flagstaff, Ariz) with partial coverage of left-subclavian artery (LSA) into the phantom aortic arch, as shown by post-operative CT imaging (Figure 1). Phantom diameter just distal the LSA was 23.6 mm so that an 11% endograft oversizing was obtained according the instruction of use (IFU) provided by Gore. Device deployment determined an excessive stent protrusion into the aortic arch (i.e., bird-beak configuration), which was characterized by a protrusion extension (PE) of 19 mm and an angle

(θ) of 24 deg between the lesser curvature of the aorta and the protruded segment of the stent-graft wall (Figure 1 B). To better explore the endograft mechanical behavior, two additional configurations were investigated with PEs of 13 mm and 24 mm, respectively.

A dynamic flow circuit, which is similar to that developed by Tsai et al. [16] to study aortic dissection, was adopted to evaluate device infolding under controlled hemodynamic conditions. In brief, the flow circuit consisted of four components: (1) a custom-made pulsatile pump, (2) the phantom model with the endograft, (3) a compliance chamber, and (4) a fluid collector, all connected by silicone tubes and plastic connectors (Figure 1 A). Two valves placed at inlet and outlet of the pulsatile pump controlled the flow from the fluid collector to the mock's loop. Stroke volume was imposed through a sinusoidal waveform with stroke time depending on systolic and diastolic duration. The perfusion fluid was a solution of 36% glycerin by volume in water to mimic blood viscosity and density. Systemic pressure was obtained varying the resistance of two adjustable valves (5) placed proximal and distal from the compliance chamber. Pressure was continuously measured at LSA by a pressure transducer (X5072 Druck, GE Measurement & Control) connected to 20G catheters (6), and thus recorded with LabVIEW software (National Instruments, Austin, TX, USA). For flow measurements, an electromagnetic flow-meter (7) (Optiflux 5300C, Krohne, Duisburg, Germany) was placed on the plastic tube after the pulsatile pump to estimate inlet flow. Flow was also measured at innominate artery and left common carotid artery by temporarily moving the flow meter from the original position and placing it on the plastic tube of these vessels. During perfusion, endograft infolding was monitored using a high resolution CMOS camera (8) (Evo8050, SVS-Vistek, Seefeld, Germany) with a Nikon Micro-Nikkor lens (AF Micro-Nikkor 60mm f/2.8D) located on the front of the

phantom. Image acquisition and post-processing were performed with the Matlab Image Acquisition Toolbox (The MathWorks, Natick, MA, USA).

Perfusion Settings

To estimate endograft infolding as input for computational modeling, three different hemodynamic scenarios with cardiac outputs of 3, 5 and 7 L/min were investigated for each bird-beak configuration (i.e., PE=13, 19 and 24 mm). This was performed due to the fact that patient-specific flow and pressure were not available. For the cardiac output of 5 L/min, a physiological flow waveform was imposed with a systemic pressure of 120/80 mmHg, systolic duration of 330 ms and heart rate of 60 bpm. Pump stroke and velocity were varied to simulate the other hemodynamic scenarios: a) a cardiac output of 3 L/m with heart rate of 60 bpm and systemic pressure of 90/55 mmHg; and b) a cardiac output of 7 L/m with 70 bpm and 170/100 mmHg. Figure 1C and D show flow and pressure profiles measured during perfusion testing. Endograft infolding was evaluated by the device displacement as defined by the displacement change of the bird-beak apex from systole to diastole. This parameter was then used to tune the computationally-derived displacement of the bird-beak configuration.

FSI Computational Modeling

The reconstructed patient-specific aortic geometry was exported to GAMBIT v2.3.6 (ANSYS Inc., Canonsburg, PA) for meshing the fluid domain (i.e, the lumen) with ~ 1 million of tetrahedral elements and the structural domain (i.e, the aorta and bird-beak endograft) with ~ 300000 quadrilateral elements. Reconstructions and meshing of the aortic anatomy were also performed for the other patients underwent TEVAR. Thus, the proximal bird-beaking was

modeled into each patient aortic arch in accordance with the values of PE measured in the post-operative CT scans.

One-way FSI analysis was performed to reproduce the fluid dynamic of experimental perfusion testing and thus to determine the mechanical forces exerted on the endograft PE [15]. Specifically, the software MpCCI v4.2 (Fraunhofer SCAI, Germany) was adopted to send the fluid solution obtained by FLUENT v14.0.0 (ANSYS Inc., Canonsburg, PA) to the structural solver, ABAQUS v6.12 (SIMULIA Inc, Providence, RI). Both codes share a common boundary surface consisting on a) the undersurface and luminal surface of the endograft PE, and b) the aortic wall. These surfaces were used for the data exchange (i.e., wall stress forces) at every time step (0.1 s) upon the total analysis time (1 s).

For the fluid model, simulations were based on an algorithm that was previously used by our group to resolve time-dependent flow instabilities encountered in complex cardiovascular anatomies [15, 17, 18]. Flow was assumed laminar, incompressible and Newtonian with density of 1060 kg/m^3 and viscosity of 0.00371 Pa x s. This is a valid assumption since low mean flow velocities usually occur in large vessels [19]. Indeed, we found a Reynolds number of 1710 just distal to the endograft PE for the Case D with the highest peak-systolic flow velocity. Boundary conditions were set using flow and pressure profiles measured experimentally. Specifically, aortic flow velocity was determined by dividing the measured aortic flow to the inlet area. Then, flow velocity was decomposed into its major harmonic mode through Fourier transformation, and a user-defined function (UDF) was generated to set the inflow profile over the cardiac cycle [20]. For both innominate artery and left common carotid artery, velocity profiles were scaled

versions of the aortic inflow with flow splits derived by the mean values of experimental data. Similarly, the measured pressure profile was fit with a polynomial function, and thus a UDF was set into LSA to mimic the experimental pressure profile.

For the structural model, the bird-beak protrusion was assumed as a linear-elastic material with Poisson's ratio of 0.3 as previously described [15]. Besides, endograft compliance was iteratively adjusted to match infolding displacements measured by experimental testing. The stent frame was not modeled so that the endograft PE was simulated as a shell with thickness of 0.9 mm. The aorta, which was 1.72 mm thick, was modeled as a hyperelastic and isotropic material using a finite strain constitutive formulation developed for modeling human aorta [21]. Distal ends of supra-aortic vessels, aortic valve and descending aorta were fixed in all directions. No-slip contact conditions were adopted to fix the interface of the endograft PE to the aortic wall.

RESULTS

Endograft displacements were found high with the more pronounced PE as compared to the short bird-beak configuration (Table 1). Additionally, infolding was found to increase from the hemodynamic scenario with systemic pressure (flow rate) of 90/55 mmHg (3 L/min) to that one with pulse pressure of 170/100 mmHg (7 L/min).

Calibration of the bird-beak mechanical parameter under different hemodynamic conditions and bird-beak configurations revealed that the endograft compliance increases with higher systemic pressure and flow rate (Figure 2). For a given hemodynamic condition, the endograft compliance linearly increases as the PE decreases. It is should be noted that the endograft compliance here

reported does not represent the Young's modulus of the endograft but rather the global endograft mechanical behavior under a particular condition of flow-induced loads (i.e, pressure exerted on both the undersurface and the luminal surface of the protruded endograft wall), geometrical configurations (i.e., combination of PE and θ), and device characteristics (i.e, features of nitinol frame).

Once endograft compliance was calibrated, FSI simulations were performed assuming a cardiac output of 5 L/min and systemic pressure of 120/80 mmHg for all patients. Figure 3 shows the pressure and velocity streamlines altered by the presence of the bird-beak configuration. Peak systolic pressure was found lower distal to the bird-beak configuration and markedly higher proximal to the ascending aorta and supra-aortic vessels [15]. This pressure drop suggests a physiologic coarctation of the aorta, resulting from the proximal protrusion of the thoracic aortic stent-graft into the arch as reported by Go and collaborators for Case A [9]. Measurements of systolic pressure across the endograft wall surface revealed a transmural pressure load difference, which increases upon 18 mmHg with the longest PE of 28mm. Table 2 shows that computationally-derived measurements of device infolding were pronounced as the PE increased from 19 mm to 26 mm, but low for the PE=28 mm (see Case D). This was likely caused by the ostium of LSA, which inhibits the endograft displacement during cardiac beating. At peak systole, streamlines run parallel to the aortic wall in the ascending aorta but those close to the protruded stent-graft wall lost this characteristic laminar pattern independently by the extension of proximal device protrusion (Figure 3). The malapposed endograft generates vortices in the proximal luminal surface of the endograft close to the tight aortic arch, and these hemodynamic disturbances are more pronounced for Case D with the greatest PE (compare Case D with Case

A). The pressure drop at LSA for Case D determined high flow velocity in correspondence of this aortic branch. Finally, intramural stress and corresponding principal strain distributions were estimated at systolic peak for all patients (Figure 4). High magnitudes of Mises stress were found in correspondence of the eight stent apices due to a stress concentration induced by the sharply-curved stent wire. Moreover, the longer the PE is the higher the Mises stress is (compare Case D with Case A). FSI analyses revealed principal strain amplitude of 0.7% for Case C, which exhibited the highest device displacement of 4.10 mm. Differently, other bird-beak configurations exhibited lower principal strain due to low device displacements (i.e., Case A and B) or anatomic constraining (Case D).

DISCUSSION

The results here presented evinced that a pronounced bird-beak protrusion into the aortic arch is the main factor contributing to the onset of a functional aortic coarctation (i.e., pressure drop) into the arch, hemodynamic disturbances in the distal descending aorta, high device displacements, elevated transmural pressure across stent-graft wall, and marked intramural stress and principal strain distributions on the endograft PE. These factors may lead to an increased risk of endograft collapse for those young patients undergoing TEVAR for traumatic aortic injuries.

Fluid dynamic studies have attempted to reveal the complex structural and hemodynamic loads exerted on the bird-beak configuration resulting from the deployment of a stent-graft into the aortic arch [15, 22-26]. Using an idealized aortic anatomy, Lam et al. [22] investigated the influence of the aortic diameter, aortic arch curvature and endograft position on the forces exerted on the endograft PE. They found that the force lifting off the bird-beak wall is

determined by a change in the momentum generated by both the blood flow and frictional forces on the graft wall. This lifting force is mainly affected by the aortic diameter and endograft position rather than the aortic arch curvature. Similarly, Cheng et al. [24] demonstrated that the lifting force depends on the graft diameter as well as the initial deployment position relative to the aortic arch of patients with TEVAR for aortic dissection. Fung et al. [25] developed a computational model to demonstrate that the principal factors contributing to device infolding are the blood pressure and pressure waveform. Specifically, a 55% increase in the lifting force was found when the systemic pressure arises from 100/70 to 180/110 mmHg. Such a finding corroborates the increased displacements of endograft PE found in our experiments as the systemic pressure was increased (see Table 1). However, these studies did not consider patient-specific aortic geometries and bird-beak configurations as well as the mechanical response of protruded stent-graft wall to the complex hemodynamic environment. As suggested by several studies [15, 23, 27], the bird-beak configuration behaves as a cantilever beam under unique conditions of flow-induced loads (i.e., a pressure difference between the luminal endograft surface and the undersurface facing the aortic arch). Such a complex loading condition and the particular endograft geometry do not permit to adopt the linear elastic theory to calculate the device displacement so that numerical simulations are needed. Therefore, the curves of endograft compliance vs PE here reported can be used to model the mechanical response of the bird-beak configurations to a given hemodynamic condition.

For all investigated patient cases, the measurements of device infolding predicted by our FSI analyses were not able to determine endograft collapse seen clinically. However, the amplitude of principal strain (see Figure 4) could cause material failure of the Nitinol stent-graft frame

under cyclic loading conditions imposed by the cardiac rhythm. Pelton and collaborators [28] estimated the fatigue properties under physiological loading deformation for Nitinol compounds extrapolated from peripheral artery stents. They reported the fatigue curve as a function of strain amplitude and found a fatigue strain limit for the Nitinol stents of 0.4%. This fatigue limit represents the strain amplitude that can be applied to the stent-graft without causing failure under compression loading conditions. In our cases, the predicted principal strains were lower than the 0.4% fatigue strain limit for Case A and D but were particularly higher for Case B and C with PEs of 21mm and 26 mm, respectively. Furthermore, device invagination due to aortic anatomic constraints cannot be considered in fatigue testing so that graft failure can occur at strain amplitude lower than that estimated by Pelton et al [28]. This suggests that endograft failure may occur due to cyclic fatigue loading conditions for all investigated patients as supported by stent-frame fractures observed after surgical repair of collapsed endografts [11, 13]. Moreover, reported collapses occurred mainly in younger patients who have elastic aortas with a more pronounced pulsatility [29], resulting in greater strain amplitude for PE. We emphasizes that these findings may be used not only to understand the putative mechanisms underlying the endograft infolding into aortic arch, but also to the design of new devices for younger individuals to be treated with an endoprosthesis for blunt traumatic aortic injury. Indeed, the new Comfortable Gore TAG device was designed using computational analysis to include modifications to the stent frame for increasing durability and compression resistance [30]. These improvements appear to have mitigated endograft collapse as reported by Gore on 10,000 implants during current clinical trials [30]. Nonetheless, the long-term durability of this new device has yet to be investigated.

Although the present study is based on the analysis of patient-specific data, there are limitations inherent to numerous anatomic and device-related variables that were not considered. The presence of a protruded endograft wall into the aorta was included indirectly through the description of its trace resulting from image segmentation. Such an approach can be certainly improved by considering the Nitinol stent frame characterizing the endograft. Nevertheless, we retain that the global mechanical behavior is well represented by our approach as confirmed in a previous FSI study [15]. Furthermore, these findings should be confined to the investigated aortic anatomies and may not be extended to other endografts because different devices have different radial force and biomechanical properties. It is however difficult to collect a large cohort of young patients with similar situations. In this study, the phantom model was obtained from a patient with a bovine arch, and this can impact the measurement of the flow-induced endograft displacement used to initially calibrate the computational model. The compliance of the silicone phantom model may differ from those occurring in the actual young aorta of the investigated patient case. The distensibility of silicone phantom allows mimicking that of a human aorta as this elastic material was used in several in-vitro models to study aortic diseases [16, 31]. However, the utilize of a patient-specific silicone phantom allowed us to study the actual aortic arch anatomy and device oversizing, which are the main contributors to endograft collapse [8, 10]. In the FSI analyses, an anisotropic constitutive formulation should better represent the real mechanical behavior of the aorta. In spite of these limitations, the present experimentally-calibrated FSI framework represents a valid tool to quantify the hemodynamic and structural loads acting on the proximal protrusion of thoracic stent grafts.

CONCLUSIONS

Length of endograft PE arising in patients underwent TEVAR can severely alter the hemodynamic and structural loads exerted on the bird-beaking. Specifically, PE leads to a functional aortic coarctation into the arch and helical flow pattern in the distal descending aorta. High device displacements and transmural pressure characterize a bird-beak configuration. Indeed, a proximal bird-beaking with a PE longer than 21 mm may lead to a considerable endograft displacement into the aortic arch, and this may warrant clinical surveillance during follow-up. Interestingly, amplitudes of principal strain observed in four young patients with different extension of PE are comparable to the fatigue strain limit reported in literature, and this suggests that endograft may collapse due to material fatigue. These findings obtained by an experimentally-calibrated FSI framework may be considered to design new devices more suitable for younger individuals, which need to be treated with an endoprosthesis for blunt traumatic aortic injury.

ACKNOWLEDGEMENTS

This research was funded by a grant from Fondazione RiMED provided to Dr. Pasta. Mr. Rinaudo acknowledges the Italian Ministry of Education, University and Research for supporting his research.

REFERENCES

[1] Criado FJ, Clark NS, Barnatan MF. Stent graft repair in the aortic arch and descending thoracic aorta: A 4-year experience. Journal of Vascular Surgery. 2002;36:1121-7.

[2] Go MR, Barbato JE, Dillavou ED, Gupta N, Rhee RY, Makaroun MS, et al. Thoracic endovascular aortic repair for traumatic aortic transection. Journal of Vascular Surgery. 2007;46:928-33.

[3] Celis RI, Park SC, Shukla AJ, Zenati MS, Chaer RA, Rhee RY, et al. Evolution of treatment for traumatic thoracic aortic injuries in a single institution J Vasc Surg. 2012;*in press*.

[4] Makaroun MS, Dillavou ED, Wheatley GH, Cambria RP, Investigators GR. Five-year results of endovascular treatment with the Gore TAG device compared with open repair of thoracic aortic aneurysms. Journal of Vascular Surgery. 2008;47:912-8.

[5] Steinbauer MG, Stehr A, Pfister K, Herold T, Zorger N, Topel I, et al. Endovascular repair of proximal endograft collapse after treatment for thoracic aortic disease. J Vasc Surg. 2006;43:609-12.

[6] Kasirajan K, Dake MD, Lumsden A, Bavaria J, Makaroun MS. Incidence and outcomes after infolding or collapse of thoracic stent grafts. J Vasc Surg. 2012;55:652-8; discussion 8.

[7] Hinchliffe RJ, Krasznai A, SchultzeKool L, Blankensteijn JD, Falkenberg M, Lonn L, et al. Observations on the failure of Stent-grafts in the aortic arch. European Journal of Vascular and Endovascular Surgery. 2007;34:451-6.

[8] Tadros RO, Lipsitz EC, Chaer RA, Faries PL, Marin ML, Cho JS. A multicenter experience of the management of collapsed thoracic endografts. Journal of Vascular Surgery. 2011.

[9] Go MR, Siegenthaler MP, Rhee RY, Gupta N, Makaroun MS, Cho JS. Physiologic coarctation of the aorta resulting from proximal protrusion of thoracic aortic stent grafts into the arch. Journal of Vascular Surgery. 2008;48:1007-11.

[10] Sze DY, Mitchell RS, Miller DC, Fleischmann D, Frisoli JK, Kee ST, et al. Infolding and collapse of thoracic endoprostheses: Manifestations and treatment options. Journal of Thoracic and Cardiovascular Surgery. 2009;138:324-33.

[11] Canaud L, Alric P, Desgranges P, Marzelle J, Marty-Ane C, Becquemin JP. Factors favoring stent-graft collapse after thoracic endovascular aortic repair. Journal of Thoracic and Cardiovascular Surgery. 2010;139:1153-7.

[12] Jonker FH, Schlosser FJ, Geirsson A, Sumpio BE, Moll FL, Muhs BE. Endograft collapse after thoracic endovascular aortic repair. J Endovasc Ther. 2010;17:725-34.

[13] Muhs BE, Balm R, White GH, Verhagen HJM. Anatomic factors associated with acute endograft collapse after Gore TAG treatment of thoracic aortic dissection or traumatic rupture. Journal of Vascular Surgery. 2007;45:655-61.

[14] Shukla AJ, Jeyabalan G, Cho JS. Late collapse of a thoracic endoprosthesis. Journal of Vascular Surgery. 2011;53:798-801.

[15] Pasta S, Cho JS, Dur O, Pekkan K, Vorp DA. Computer modeling for the prediction of thoracic aortic stent graft collapse. Journal of Vascular Surgery. 2013;57:1353-61.

[16] Tsai TT, Schlicht MS, Khanafer K, Bull JL, Valassis DT, Williams DM, et al. Tear size and location impacts false lumen pressure in an ex vivo model of chronic type B aortic dissection. J Vasc Surg. 2008;47:844-51.

[17] Pasta S, Rinaudo A, Luca A, Pilato M, Scardulla C, Gleason TG, et al. Difference in hemodynamic and wall stress of ascending thoracic aortic aneurysms with bicuspid and tricuspid aortic valve. J Biomech. 2013;46:1729-38.

[18] D'Ancona G, Lee JJ, Pasta S, Pilato G, Rinaudo A, Follis F, et al. Computational analysis to predict false-lumen perfusion and outcome of type B aortic dissection. J Thorac Cardiovasc Surg. 2014;148:1756-8.

[19] Morris L, Delassus P, Walsh M, McGloughlin T. A mathematical model to predict the in vivo pulsatile drag forces acting on bifurcated stent grafts used in endovascular treatment of abdominal aortic aneurysms (AAA). J Biomech. 2004;37:1087-95.

[20] Dur O, DeGroff CG, Keller BB, Pekkan K. Optimization of Inflow Waveform Phase-Difference for Minimized Total Cavopulmonary Power Loss. Journal of Biomechanical Engineering-Transactions of the Asme. 2010;132:-.

[21] Raghavan ML, Vorp DA. Toward a biomechanical tool to evaluate rupture potential of abdominal aortic aneurysm: identification of a finite strain constitutive model and evaluation of its applicability. Journal of Biomechanics. 2000;33:475-82.

[22] Lam SK, Fung GS, Cheng SW, Chow KW. A computational study on the biomechanical factors related to stent-graft models in the thoracic aorta. Med Biol Eng Comput. 2008;46:1129-38.

[23] van Bogerijen GH, Auricchio F, Conti M, Lefieux A, Reali A, Veneziani A, et al. Aortic hemodynamics after thoracic endovascular aortic repair, with particular attention to the bird-beak configuration. J Endovasc Ther. 2014;21:791-802.

[24] Cheng SW, Lam ES, Fung GS, Ho P, Ting AC, Chow KW. A computational fluid dynamic study of stent graft remodeling after endovascular repair of thoracic aortic dissections. J Vasc Surg. 2008;48:303-9; discusion 9-10.

[25] Fung GS, Lam SK, Cheng SW, Chow KW. On stent-graft models in thoracic aortic endovascular repair: a computational investigation of the hemodynamic factors. Computers in biology and medicine. 2008;38:484-9.

[26] Auricchio F, Conti M, Marconi S, Reali A, Tolenaar JL, Trimarchi S. Patient-specific aortic endografting simulation: from diagnosis to prediction. Computers in biology and medicine. 2013;43:386-94.

[27] Auricchio F, Conti M, Lefieux A, Morganti S, Reali A, Sardanelli F, et al. Patient-specific analysis of post-operative aortic hemodynamics: a focus on thoracic endovascular repair (TEVAR). Comput Mech. 2014;54:943-53.

[28] Pelton AR, Schroeder V, Mitchell MR, Gong XY, Barney M, Robertson SW. Fatigue and durability of Nitinol stents. Journal of the mechanical behavior of biomedical materials. 2008;1:153-64.

[29] Leung DA, Davis I, Katlaps G, Tisnado J, Sydnor MK, Komorowski DJ, et al. Treatment of infolding related to the gore TAG thoracic endoprosthesis. Journal of vascular and interventional radiology : JVIR. 2008;19:600-5.

[30] Farber MA, Giglia JS, Starnes BW, Stevens SL, Holleman J, Chaer R, et al. Evaluation of the redesigned conformable GORE TAG thoracic endoprosthesis for traumatic aortic transection. J Vasc Surg. 2013;58:651-8.

[31] Rudenick PA, Bijnens BH, Garcia-Dorado D, Evangelista A. An in vitro phantom study on the influence of tear size and configuration on the hemodynamics of the lumina in chronic type B aortic dissections. J Vasc Surg. 2013;57:464-74 e5.

Figure Legends

Figure 1: (A) Schematic of pulsatile flow circuit; (B) photography of phantom model with particulars of bird-beak configurations with PE=19 mm; (C) pressure profiles measured for bird-beak configuration with PE=19 mm and θ =20 deg at different cardiac outputs; (D) flow profiles measured at aortic inlet. The accuracy of infolding measurement was 29 μm for a field of view of 30 x 35 mm with images acquired at 30 fps.

Figure 2: TAG compliance profiles obtained after interative (manual) calibration of infolding parameters for the investigated hemodynamic scenarios (R^2>0.96 for all fitting curves)

Figure 3: Pressure distribution (row above) and velocity streamlines (row below) at systolic peak for all patients with a protruded endograft wall; Case A with PE=19mm; Case B with PE=21mm; Case C with PE=26mm; Case D with PE=28mm

Figure 4: Distributions of Mises's stress (row above) and strain (row below) of the protruded endograft walls estimated at peak of systole; Case A with PE=19mm; Case B with PE=21mm; Case C with PE=26mm; Case D with PE=28mm

Table 1: TAG device displacements experimentally measured under different perfusion conditions.

	TAG Device Displacement (mm)		
	ΔP=90/55mmHg; CO=3L/min	ΔP=120/80mmHg; CO=5L/min	ΔP=170/100mmHg; CO=7L/min
PE=13mm	0.26	0.39	0.65
PE=19mm	0.60	0.89	1.20
PE=24mm	0.72	1.01	1.66

Note: DP: systemic pressure; CO: cardiac output

Table 2: Transmural pressure across the protruded endograft wall and endograft displacements for all patients; Case A with PE=19mm; Case B with PE=21mm; Case C with PE=26mm; Case D with PE=28mm

	Case A	Case B	Case C	Case D
Transmural Pressure (mmHg)	0.89	1.26	2.85	8.72
Endograft Displacement (mm)	0.89	1.18	4.10	3.15

Fig 1

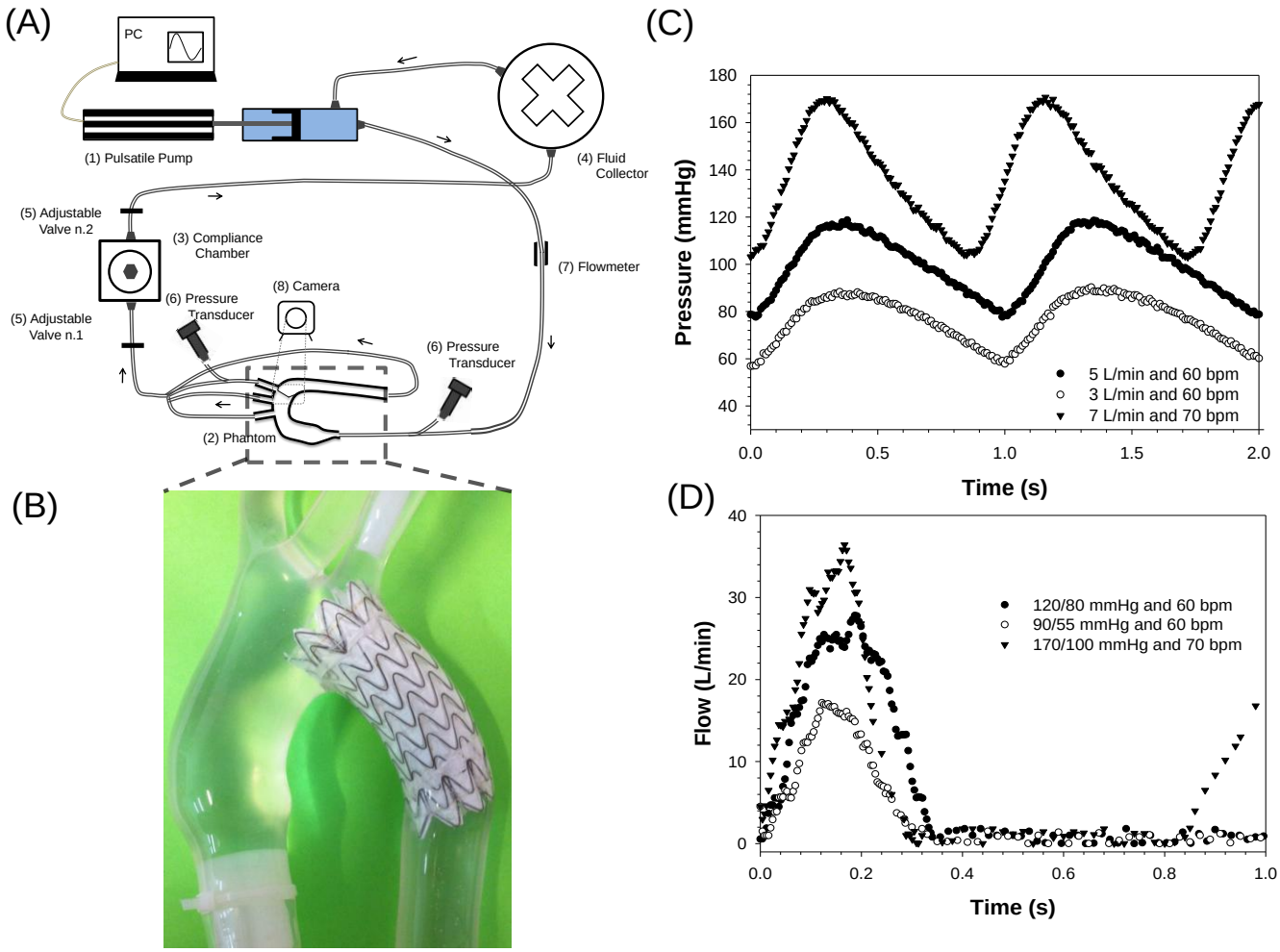
(A)
PC
(1) Pulsatile Pump
(4) Fluid Collector
(5) Adjustable Valve n.2
(3) Compliance Chamber
(7) Flowmeter
(6) Pressure Transducer
(8) Camera
(5) Adjustable Valve n.1
(6) Pressure Transducer
(2) Phantom
(B)
(C)
Pressure (mmHg)
Time (s)
5 L/min and 60 bpm
3 L/min and 60 bpm
7 L/min and 70 bpm
(D)
Flow (L/min)
Time (s)
120/80 mmHg and 60 bpm
90/55 mmHg and 60 bpm
170/100 mmHg and 70 bpm

Fig 2

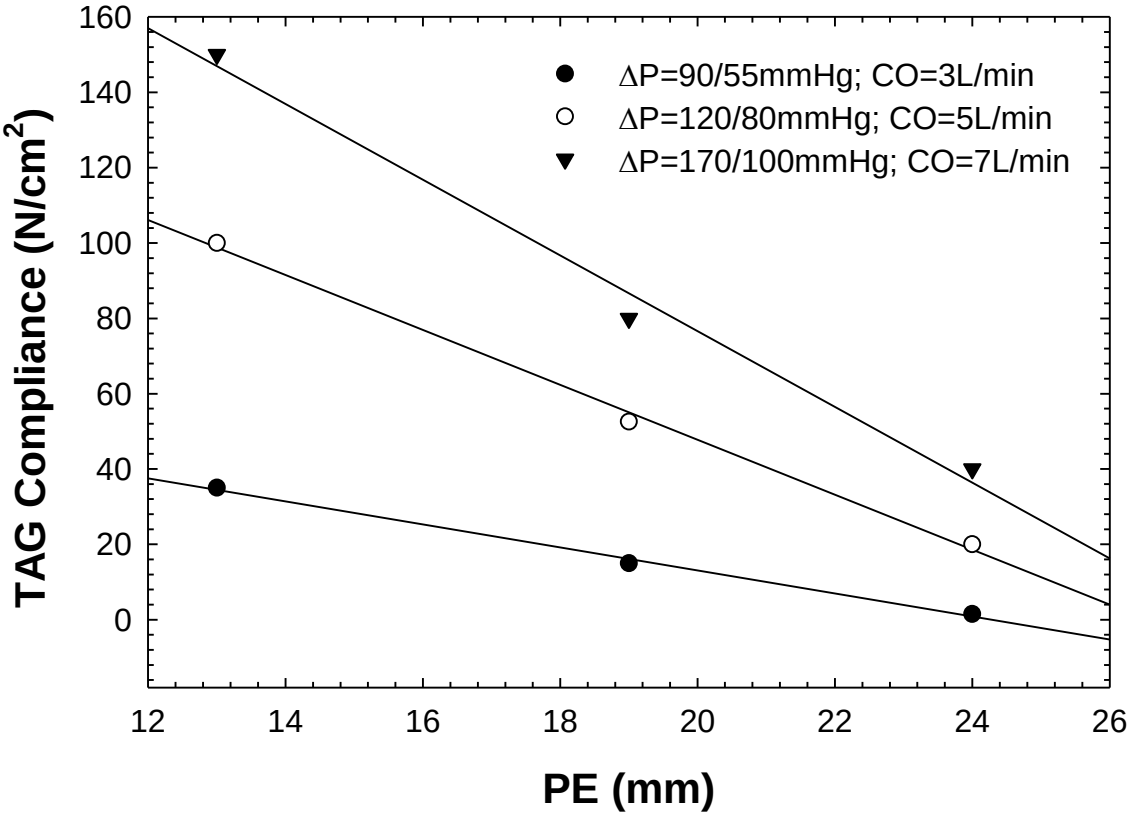
TAG Compliance (N/cm2)
PE (mm)
ΔP=90/55mmHg; CO=3L/min
ΔP=120/80mmHg; CO=5L/min
ΔP=170/100mmHg; CO=7L/min
160
140
120
100
80
60
40
20
0
12
14
16
18
20
22
24
26

Fig 3

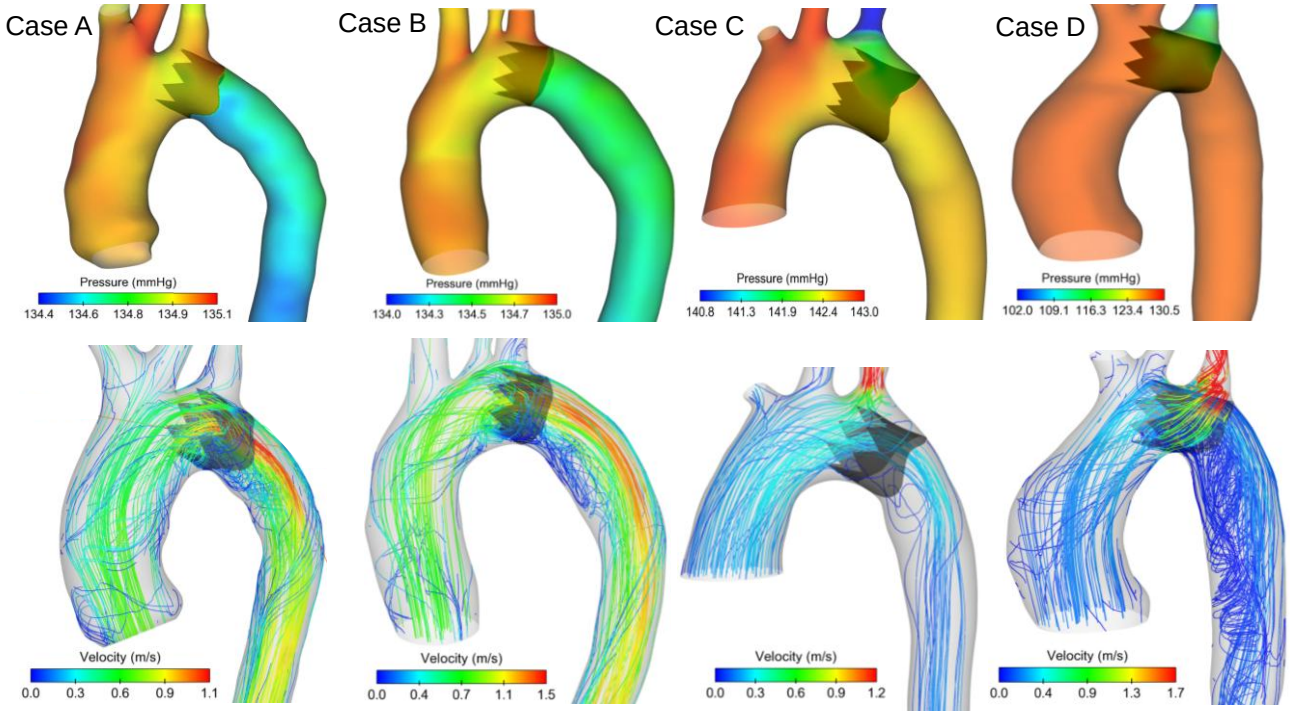
Case A
Case B
Case C
Case D
Pressure (mmHg)
134.4 134.6 134.8 134.9 135.1
Pressure (mmHg)
134.0 134.3 134.5 134.7 135.0
Pressure (mmHg)
140.8 141.3 141.9 142.4 143.0
Pressure (mmHg)
102.0 109.1 116.3 123.4 130.5
Velocity (m/s)
0.0 0.3 0.6 0.9 1.1
Velocity (m/s)
0.0 0.4 0.7 1.1 1.5
Velocity (m/s)
0.0 0.3 0.6 0.9 1.2
Velocity (m/s)
0.0 0.4 0.9 1.3 1.7

Fig 4

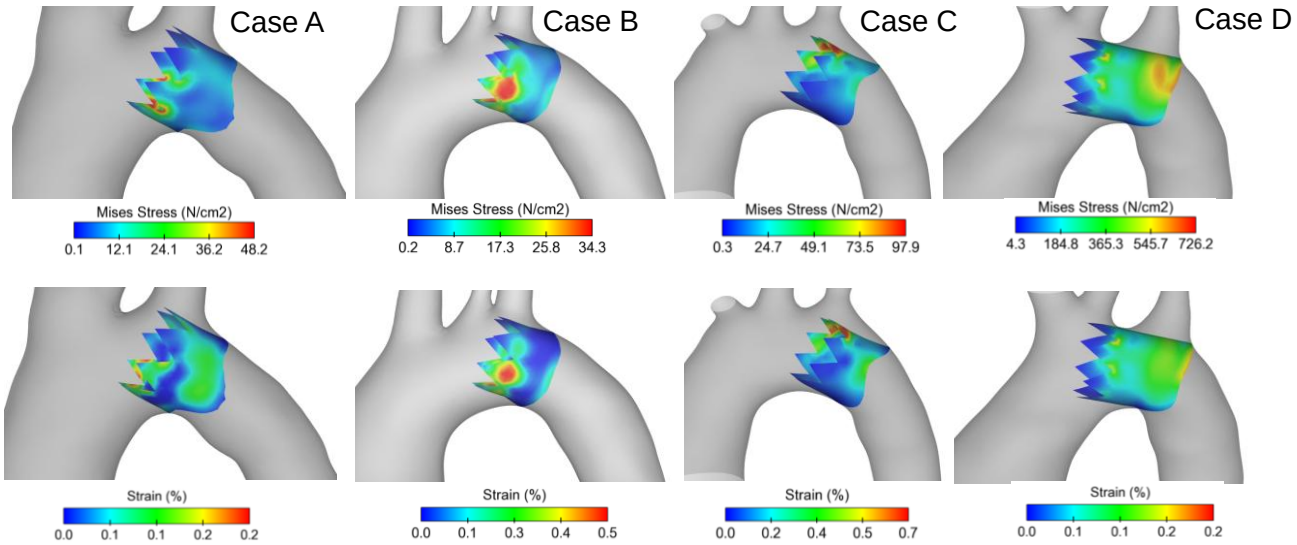
Case A
Case B
Case C
Case D
Mises Stress (N/cm2)
0.1 12.1 24.1 36.2 48.2
Mises Stress (N/cm2)
0.2 8.7 17.3 25.8 34.3
Mises Stress (N/cm2)
0.3 24.7 49.1 73.5 97.9
Mises Stress (N/cm2)
4.3 184.8 365.3 545.7 726.2
Strain (%)
0.0 0.1 0.1 0.2 0.2
Strain (%)
0.0 0.1 0.3 0.4 0.5
Strain (%)
0.0 0.2 0.4 0.5 0.7
Strain (%)
0.0 0.1 0.1 0.2 0.2

Biomechanical Implications of Excessive Endograft Protrusion into the Aortic Arch after Thoracic Endovascular Repair

Antonino Rinaudo[1], Giuseppe Maria Raffa[2], Francesco Scardulla[1],
Michele Pilato[2], Cesare Scardulla[2], Salvatore Pasta[2,3]

[1] DICGIM, Universitá di Palermo, Palermo, Italy

[2] Department for the Treatment and Study of Cardiothoracic Diseases and Cardiothoracic Transplantation, Mediterranean Institute for Transplantation and Advanced Specialized Therapies (ISMETT), Palermo, Italy

[3] Fondazione Ri.MED, Palermo, Italy

Conflict of Interest: none

Sources of Financial Support: RiMED Foundation

Corresponding author:
Salvatore Pasta, PhD
NSQ Professor in Mechanical Engineering
Fondazione Ri.MED
Cell: +39 3349379694
Phone: +39 091 6041 111
FAX: +39 091 6041 122
e-mail: spasta@fondazionerimed.com

ABSTRACT

Endografts placed in the aorta for thoracic endovascular aortic repair (TEVAR) may determine malappositioning to the lesser curvature of the aortic wall, thus resulting in a devastating complication known as endograft collapse. This premature device failure commonly occurs in young individuals after TEVAR for traumatic aortic injuries as a result of applications outside the physical conditions for which the endograft was designed. In this study, an experimentally-calibrated fluid-structure interaction (FSI) model was developed to assess the hemodynamic and stress/strain distributions acting on the excessive protrusion extension (PE) of endografts deployed in four young patients underwent TEVAR. Endograft infolding was experimentally measured for different hemodynamic scenarios by perfusion testing and then used to numerically calibrate the mechanical behavior of endograft PE. Results evinced that the extent of endograft can severely alter the hemodynamic and structural loads exerted on the endograft PE. Specifically, PE determined a physiological aortic coarctation into the aortic arch characterized by a helical flow in the distal descending aorta. High device displacement and transmural pressure across the stent-graft wall were found for a PE longer than 21 mm. Finally, marked intramural stress and principal strain distributions on the protruded segment of the endograft wall may suggest failure due to material fatigue. These critical parameters may contribute to the endograft collapse observed clinically and can be used to design new devices more suitable for young individuals to be treated with an endoprosthesis for TEVAR of blunt traumatic aortic injuries.

Key words: thoracic endovascular aortic repair (TEVAR), bird-beak, stent-graft, endograft collapse/infolding; fluid-structure interaction

INTRODUCTION

Thoracic endovascular aortic repair (TEVAR) has emerged over the last decade as the preferential minimally invasive therapeutic modality for a variety of thoracic aortic pathologies, including traumatic thoracic aortic injuries [1-3]. TEVAR for traumatic injuries is effective but its outcome remains a concern especially in young patients [4, 5]. In these individuals, the endograft is often implanted "off-label", and device oversizing is essential for fixation at the level of the proximal landing zone [6]. This may ultimately induce to premature device failure and endograft collapse/infolding, which usually requires a secondary intervention by means of re-do TEVAR or conversion to open surgery with attendant high morbidity and mortality [7-10]. The incidence rates of endograft collapse after TEVAR for traumatic injuries are not well defined [8, 11], although collapses usually present in the early post-operative period (median time of 15 days) [12]. It has been recently reported that the Gore TAG thoracic endoprosthesis (W. L. Gore and Assoc, Flagstaff, Ariz) accumulated a 0.4% frequency rate of device collapse among 33,000 endografts distributed worldwide [6]. However, collapse rates likely differ for other available endografts.

A number of anatomic- and device-related factors may contribute to endograft infolding including a young healthy aorta with tight aortic arch and marked pulsatility, excessive stent-graft oversizing and material fatigue [8, 12, 13]. Endograft infolding–related mortality rates of 16.9% for asymptomatic patients and 27.3% for symptomatic patients within 3 years of diagnosis [11, 13, 14]. Collapses are most often observed when the proximal extent of the endograft is in the transverse arch with malapposition of the endograft wall along the lesser curvature of the aorta (the so-called "bird-beak" phenomenon) [9-11, 14]. Bird-beaking is not desirable because it

exposes the graft undersurface to the force of the bloodstream. However, the bird-beak configuration is not the only determinant of stent-graft collapse, because this phenomenon has not been observed with high frequency in patients with thoracic aneurysms (10.1% of 139 TAG collapses), many of whom can present a proximal bird-beaking in the aortic arch [6].

Although the bird-beak effect is often observed after TEVAR of traumatic injuries in young patients [11], collapses do not occur in all of them. It would be also desirable if these individuals with increased risk for developing such a complication would benefit of ad-hoc endografts to tailor their tight and elastic aortic arch. However, the mechanics of endograft collapse has not been clearly defined yet. The understanding of the mechanisms underlying endograft collapse may lead to the design of new devices for TEVAR in young patients. Therefore, we developed an experimentally-calibrated computational model to study the hemodynamic, wall stress and strain acting on the bird-beak configuration observed in four patients underwent TEVAR. Initially, endograft infolding was measured for different perfusion conditions and bird-beak configurations in a patient-specific phantom model. Then, infolding measurements were used as input for a fluid-structure interaction (FSI) model to tune the endograft mechanical property and then the displacement of the proximal protruded wall of the endograft. Finally, computational simulations were performed to estimate the intramural wall stress and principal strain distributions on the bird-beaking of four young patients underwent TEVAR for traumatic thoracic aortic injuries. The possible causes of endograft collapse are discussed.

METHODS

The role of hemodynamic loads on the infolding resulting from the bird-beak configuration of a thoracic endograft was explored using a case of a male patient who underwent TEVAR for a traumatic aortic injury, and subsequently developed stent-graft collapse with neurologic complications, as previously investigated by our group [14]. Once a phantom model of the patient aortic anatomy was obtained, the infolding resulting from the endograft deployment was assessed by perfusion testing and then used to calibrate the global mechanical behavior of the endograft implanted in this patient. Finally, the hemodynamic and the strain/stress distributions on the protruded stent-graft wall were predicted for four young patients with mean age of 32±9 yrs.

Phantom and Flow Circuit

To reconstruct the aortic geometry after TEVAR, the post-operative patient's CT scan was segmented using the vascular modeling toolkit VMTK as previously described [15]. Thus, the reconstructed patient-specific aortic geometry was transferred to the Metal Professional (River Road, WI, USA) in order to manufacture a compliant and transparent silicone phantom model. The latter represents a scale 1:1 of the patient's aortic anatomy after endovascular repair. Under no perfusion conditions, scissor-handle forceps were utilized to deploy a 26 mm x 10 cm Gore TAG thoracic endoprosthesis (TAG v1.5, W. L. Gore and Assoc, Flagstaff, Ariz) with partial coverage of left-subclavian artery (LSA) into the phantom aortic arch, as shown by post-operative CT imaging (Figure 1). Phantom diameter just distal the LSA was 23.6 mm so that an 11% endograft oversizing was obtained according the instruction of use (IFU) provided by Gore. Device deployment determined an excessive stent protrusion into the aortic arch (i.e., bird-beak configuration), which was characterized by a protrusion extension (PE) of 19 mm and an angle

(θ) of 24 deg between the lesser curvature of the aorta and the protruded segment of the stent-graft wall (Figure 1 B). To better explore the endograft mechanical behavior, two additional configurations were investigated with PEs of 13 mm and 24 mm, respectively.

A dynamic flow circuit, which is similar to that developed by Tsai et al. [16] to study aortic dissection, was adopted to evaluate device infolding under controlled hemodynamic conditions. In brief, the flow circuit consisted of four components: (1) a custom-made pulsatile pump, (2) the phantom model with the endograft, (3) a compliance chamber, and (4) a fluid collector, all connected by silicone tubes and plastic connectors (Figure 1 A). Two valves placed at inlet and outlet of the pulsatile pump controlled the flow from the fluid collector to the mock's loop. Stroke volume was imposed through a sinusoidal waveform with stroke time depending on systolic and diastolic duration. The perfusion fluid was a solution of 36% glycerin by volume in water to mimic blood viscosity and density. Systemic pressure was obtained varying the resistance of two adjustable valves (5) placed proximal and distal from the compliance chamber. Pressure was continuously measured at LSA by a pressure transducer (X5072 Druck, GE Measurement & Control) connected to 20G catheters (6), and thus recorded with LabVIEW software (National Instruments, Austin, TX, USA). For flow measurements, an electromagnetic flow-meter (7) (Optiflux 5300C, Krohne, Duisburg, Germany) was placed on the plastic tube after the pulsatile pump to estimate inlet flow. Flow was also measured at innominate artery and left common carotid artery by temporarily moving the flow meter from the original position and placing it on the plastic tube of these vessels. During perfusion, endograft infolding was monitored using a high resolution CMOS camera (8) (Evo8050, SVS-Vistek, Seefeld, Germany) with a Nikon Micro-Nikkor lens (AF Micro-Nikkor 60mm f/2.8D) located on the front of the

phantom. Image acquisition and post-processing were performed with the Matlab Image Acquisition Toolbox (The MathWorks, Natick, MA, USA).

Perfusion Settings

To estimate endograft infolding as input for computational modeling, three different hemodynamic scenarios with cardiac outputs of 3, 5 and 7 L/min were investigated for each bird-beak configuration (i.e., PE=13, 19 and 24 mm). This was performed due to the fact that patient-specific flow and pressure were not available. For the cardiac output of 5 L/min, a physiological flow waveform was imposed with a systemic pressure of 120/80 mmHg, systolic duration of 330 ms and heart rate of 60 bpm. Pump stroke and velocity were varied to simulate the other hemodynamic scenarios: a) a cardiac output of 3 L/m with heart rate of 60 bpm and systemic pressure of 90/55 mmHg; and b) a cardiac output of 7 L/m with 70 bpm and 170/100 mmHg. Figure 1C and D show flow and pressure profiles measured during perfusion testing. Endograft infolding was evaluated by the device displacement as defined by the displacement change of the bird-beak apex from systole to diastole. This parameter was then used to tune the computationally-derived displacement of the bird-beak configuration.

FSI Computational Modeling

The reconstructed patient-specific aortic geometry was exported to GAMBIT v2.3.6 (ANSYS Inc., Canonsburg, PA) for meshing the fluid domain (i.e, the lumen) with ~ 1 million of tetrahedral elements and the structural domain (i.e, the aorta and bird-beak endograft) with ~ 300000 quadrilateral elements. Reconstructions and meshing of the aortic anatomy were also performed for the other patients underwent TEVAR. Thus, the proximal bird-beaking was

modeled into each patient aortic arch in accordance with the values of PE measured in the post-operative CT scans.

One-way FSI analysis was performed to reproduce the fluid dynamic of experimental perfusion testing and thus to determine the mechanical forces exerted on the endograft PE [15]. Specifically, the software MpCCI v4.2 (Fraunhofer SCAI, Germany) was adopted to send the fluid solution obtained by FLUENT v14.0.0 (ANSYS Inc., Canonsburg, PA) to the structural solver, ABAQUS v6.12 (SIMULIA Inc, Providence, RI). Both codes share a common boundary surface consisting on a) the undersurface and luminal surface of the endograft PE, and b) the aortic wall. These surfaces were used for the data exchange (i.e., wall stress forces) at every time step (0.1 s) upon the total analysis time (1 s).

For the fluid model, simulations were based on an algorithm that was previously used by our group to resolve time-dependent flow instabilities encountered in complex cardiovascular anatomies [15, 17, 18]. Flow was assumed laminar, incompressible and Newtonian with density of 1060 kg/m^3 and viscosity of 0.00371 Pa x s. This is a valid assumption since low mean flow velocities usually occur in large vessels [19]. Indeed, we found a Reynolds number of 1710 just distal to the endograft PE for the Case D with the highest peak-systolic flow velocity. Boundary conditions were set using flow and pressure profiles measured experimentally. Specifically, aortic flow velocity was determined by dividing the measured aortic flow to the inlet area. Then, flow velocity was decomposed into its major harmonic mode through Fourier transformation, and a user-defined function (UDF) was generated to set the inflow profile over the cardiac cycle [20]. For both innominate artery and left common carotid artery, velocity profiles were scaled

versions of the aortic inflow with flow splits derived by the mean values of experimental data. Similarly, the measured pressure profile was fit with a polynomial function, and thus a UDF was set into LSA to mimic the experimental pressure profile.

For the structural model, the bird-beak protrusion was assumed as a linear-elastic material with Poisson's ratio of 0.3 as previously described [15]. Besides, endograft compliance was iteratively adjusted to match infolding displacements measured by experimental testing. The stent frame was not modeled so that the endograft PE was simulated as a shell with thickness of 0.9 mm. The aorta, which was 1.72 mm thick, was modeled as a hyperelastic and isotropic material using a finite strain constitutive formulation developed for modeling human aorta [21]. Distal ends of supra-aortic vessels, aortic valve and descending aorta were fixed in all directions. No-slip contact conditions were adopted to fix the interface of the endograft PE to the aortic wall.

RESULTS

Endograft displacements were found high with the more pronounced PE as compared to the short bird-beak configuration (Table 1). Additionally, infolding was found to increase from the hemodynamic scenario with systemic pressure (flow rate) of 90/55 mmHg (3 L/min) to that one with pulse pressure of 170/100 mmHg (7 L/min).

Calibration of the bird-beak mechanical parameter under different hemodynamic conditions and bird-beak configurations revealed that the endograft compliance increases with higher systemic pressure and flow rate (Figure 2). For a given hemodynamic condition, the endograft compliance linearly increases as the PE decreases. It is should be noted that the endograft compliance here

reported does not represent the Young's modulus of the endograft but rather the global endograft mechanical behavior under a particular condition of flow-induced loads (i.e, pressure exerted on both the undersurface and the luminal surface of the protruded endograft wall), geometrical configurations (i.e., combination of PE and θ), and device characteristics (i.e, features of nitinol frame).

Once endograft compliance was calibrated, FSI simulations were performed assuming a cardiac output of 5 L/min and systemic pressure of 120/80 mmHg for all patients. Figure 3 shows the pressure and velocity streamlines altered by the presence of the bird-beak configuration. Peak systolic pressure was found lower distal to the bird-beak configuration and markedly higher proximal to the ascending aorta and supra-aortic vessels [15]. This pressure drop suggests a physiologic coarctation of the aorta, resulting from the proximal protrusion of the thoracic aortic stent-graft into the arch as reported by Go and collaborators for Case A [9]. Measurements of systolic pressure across the endograft wall surface revealed a transmural pressure load difference, which increases upon 18 mmHg with the longest PE of 28mm. Table 2 shows that computationally-derived measurements of device infolding were pronounced as the PE increased from 19 mm to 26 mm, but low for the PE=28 mm (see Case D). This was likely caused by the ostium of LSA, which inhibits the endograft displacement during cardiac beating. At peak systole, streamlines run parallel to the aortic wall in the ascending aorta but those close to the protruded stent-graft wall lost this characteristic laminar pattern independently by the extension of proximal device protrusion (Figure 3). The malapposed endograft generates vortices in the proximal luminal surface of the endograft close to the tight aortic arch, and these hemodynamic disturbances are more pronounced for Case D with the greatest PE (compare Case D with Case

A). The pressure drop at LSA for Case D determined high flow velocity in correspondence of this aortic branch. Finally, intramural stress and corresponding principal strain distributions were estimated at systolic peak for all patients (Figure 4). High magnitudes of Mises stress were found in correspondence of the eight stent apices due to a stress concentration induced by the sharply-curved stent wire. Moreover, the longer the PE is the higher the Mises stress is (compare Case D with Case A). FSI analyses revealed principal strain amplitude of 0.7% for Case C, which exhibited the highest device displacement of 4.10 mm. Differently, other bird-beak configurations exhibited lower principal strain due to low device displacements (i.e., Case A and B) or anatomic constraining (Case D).

DISCUSSION

The results here presented evinced that a pronounced bird-beak protrusion into the aortic arch is the main factor contributing to the onset of a functional aortic coarctation (i.e., pressure drop) into the arch, hemodynamic disturbances in the distal descending aorta, high device displacements, elevated transmural pressure across stent-graft wall, and marked intramural stress and principal strain distributions on the endograft PE. These factors may lead to an increased risk of endograft collapse for those young patients undergoing TEVAR for traumatic aortic injuries.

Fluid dynamic studies have attempted to reveal the complex structural and hemodynamic loads exerted on the bird-beak configuration resulting from the deployment of a stent-graft into the aortic arch [15, 22-26]. Using an idealized aortic anatomy, Lam et al. [22] investigated the influence of the aortic diameter, aortic arch curvature and endograft position on the forces exerted on the endograft PE. They found that the force lifting off the bird-beak wall is

determined by a change in the momentum generated by both the blood flow and frictional forces on the graft wall. This lifting force is mainly affected by the aortic diameter and endograft position rather than the aortic arch curvature. Similarly, Cheng et al. [24] demonstrated that the lifting force depends on the graft diameter as well as the initial deployment position relative to the aortic arch of patients with TEVAR for aortic dissection. Fung et al. [25] developed a computational model to demonstrate that the principal factors contributing to device infolding are the blood pressure and pressure waveform. Specifically, a 55% increase in the lifting force was found when the systemic pressure arises from 100/70 to 180/110 mmHg. Such a finding corroborates the increased displacements of endograft PE found in our experiments as the systemic pressure was increased (see Table 1). However, these studies did not consider patient-specific aortic geometries and bird-beak configurations as well as the mechanical response of protruded stent-graft wall to the complex hemodynamic environment. As suggested by several studies [15, 23, 27], the bird-beak configuration behaves as a cantilever beam under unique conditions of flow-induced loads (i.e., a pressure difference between the luminal endograft surface and the undersurface facing the aortic arch). Such a complex loading condition and the particular endograft geometry do not permit to adopt the linear elastic theory to calculate the device displacement so that numerical simulations are needed. Therefore, the curves of endograft compliance vs PE here reported can be used to model the mechanical response of the bird-beak configurations to a given hemodynamic condition.

For all investigated patient cases, the measurements of device infolding predicted by our FSI analyses were not able to determine endograft collapse seen clinically. However, the amplitude of principal strain (see Figure 4) could cause material failure of the Nitinol stent-graft frame

under cyclic loading conditions imposed by the cardiac rhythm. Pelton and collaborators [28] estimated the fatigue properties under physiological loading deformation for Nitinol compounds extrapolated from peripheral artery stents. They reported the fatigue curve as a function of strain amplitude and found a fatigue strain limit for the Nitinol stents of 0.4%. This fatigue limit represents the strain amplitude that can be applied to the stent-graft without causing failure under compression loading conditions. In our cases, the predicted principal strains were lower than the 0.4% fatigue strain limit for Case A and D but were particularly higher for Case B and C with PEs of 21mm and 26 mm, respectively. Furthermore, device invagination due to aortic anatomic constraints cannot be considered in fatigue testing so that graft failure can occur at strain amplitude lower than that estimated by Pelton et al [28]. This suggests that endograft failure may occur due to cyclic fatigue loading conditions for all investigated patients as supported by stent-frame fractures observed after surgical repair of collapsed endografts [11, 13]. Moreover, reported collapses occurred mainly in younger patients who have elastic aortas with a more pronounced pulsatility [29], resulting in greater strain amplitude for PE. We emphasizes that these findings may be used not only to understand the putative mechanisms underlying the endograft infolding into aortic arch, but also to the design of new devices for younger individuals to be treated with an endoprosthesis for blunt traumatic aortic injury. Indeed, the new Comfortable Gore TAG device was designed using computational analysis to include modifications to the stent frame for increasing durability and compression resistance [30]. These improvements appear to have mitigated endograft collapse as reported by Gore on 10,000 implants during current clinical trials [30]. Nonetheless, the long-term durability of this new device has yet to be investigated.

Although the present study is based on the analysis of patient-specific data, there are limitations inherent to numerous anatomic and device-related variables that were not considered. The presence of a protruded endograft wall into the aorta was included indirectly through the description of its trace resulting from image segmentation. Such an approach can be certainly improved by considering the Nitinol stent frame characterizing the endograft. Nevertheless, we retain that the global mechanical behavior is well represented by our approach as confirmed in a previous FSI study [15]. Furthermore, these findings should be confined to the investigated aortic anatomies and may not be extended to other endografts because different devices have different radial force and biomechanical properties. It is however difficult to collect a large cohort of young patients with similar situations. In this study, the phantom model was obtained from a patient with a bovine arch, and this can impact the measurement of the flow-induced endograft displacement used to initially calibrate the computational model. The compliance of the silicone phantom model may differ from those occurring in the actual young aorta of the investigated patient case. The distensibility of silicone phantom allows mimicking that of a human aorta as this elastic material was used in several in-vitro models to study aortic diseases [16, 31]. However, the utilize of a patient-specific silicone phantom allowed us to study the actual aortic arch anatomy and device oversizing, which are the main contributors to endograft collapse [8, 10]. In the FSI analyses, an anisotropic constitutive formulation should better represent the real mechanical behavior of the aorta. In spite of these limitations, the present experimentally-calibrated FSI framework represents a valid tool to quantify the hemodynamic and structural loads acting on the proximal protrusion of thoracic stent grafts.

CONCLUSIONS

Length of endograft PE arising in patients underwent TEVAR can severely alter the hemodynamic and structural loads exerted on the bird-beaking. Specifically, PE leads to a functional aortic coarctation into the arch and helical flow pattern in the distal descending aorta. High device displacements and transmural pressure characterize a bird-beak configuration. Indeed, a proximal bird-beaking with a PE longer than 21 mm may lead to a considerable endograft displacement into the aortic arch, and this may warrant clinical surveillance during follow-up. Interestingly, amplitudes of principal strain observed in four young patients with different extension of PE are comparable to the fatigue strain limit reported in literature, and this suggests that endograft may collapse due to material fatigue. These findings obtained by an experimentally-calibrated FSI framework may be considered to design new devices more suitable for younger individuals, which need to be treated with an endoprosthesis for blunt traumatic aortic injury.

ACKNOWLEDGEMENTS

This research was funded by a grant from Fondazione RiMED provided to Dr. Pasta. Mr. Rinaudo acknowledges the Italian Ministry of Education, University and Research for supporting his research.

REFERENCES

[1] Criado FJ, Clark NS, Barnatan MF. Stent graft repair in the aortic arch and descending thoracic aorta: A 4-year experience. Journal of Vascular Surgery. 2002;36:1121-7.

[2] Go MR, Barbato JE, Dillavou ED, Gupta N, Rhee RY, Makaroun MS, et al. Thoracic endovascular aortic repair for traumatic aortic transection. Journal of Vascular Surgery. 2007;46:928-33.

[3] Celis RI, Park SC, Shukla AJ, Zenati MS, Chaer RA, Rhee RY, et al. Evolution of treatment for traumatic thoracic aortic injuries in a single institution J Vasc Surg. 2012;*in press*.

[4] Makaroun MS, Dillavou ED, Wheatley GH, Cambria RP, Investigators GR. Five-year results of endovascular treatment with the Gore TAG device compared with open repair of thoracic aortic aneurysms. Journal of Vascular Surgery. 2008;47:912-8.

[5] Steinbauer MG, Stehr A, Pfister K, Herold T, Zorger N, Topel I, et al. Endovascular repair of proximal endograft collapse after treatment for thoracic aortic disease. J Vasc Surg. 2006;43:609-12.

[6] Kasirajan K, Dake MD, Lumsden A, Bavaria J, Makaroun MS. Incidence and outcomes after infolding or collapse of thoracic stent grafts. J Vasc Surg. 2012;55:652-8; discussion 8.

[7] Hinchliffe RJ, Krasznai A, SchultzeKool L, Blankensteijn JD, Falkenberg M, Lonn L, et al. Observations on the failure of Stent-grafts in the aortic arch. European Journal of Vascular and Endovascular Surgery. 2007;34:451-6.

[8] Tadros RO, Lipsitz EC, Chaer RA, Faries PL, Marin ML, Cho JS. A multicenter experience of the management of collapsed thoracic endografts. Journal of Vascular Surgery. 2011.

[9] Go MR, Siegenthaler MP, Rhee RY, Gupta N, Makaroun MS, Cho JS. Physiologic coarctation of the aorta resulting from proximal protrusion of thoracic aortic stent grafts into the arch. Journal of Vascular Surgery. 2008;48:1007-11.

[10] Sze DY, Mitchell RS, Miller DC, Fleischmann D, Frisoli JK, Kee ST, et al. Infolding and collapse of thoracic endoprostheses: Manifestations and treatment options. Journal of Thoracic and Cardiovascular Surgery. 2009;138:324-33.

[11] Canaud L, Alric P, Desgranges P, Marzelle J, Marty-Ane C, Becquemin JP. Factors favoring stent-graft collapse after thoracic endovascular aortic repair. Journal of Thoracic and Cardiovascular Surgery. 2010;139:1153-7.

[12] Jonker FH, Schlosser FJ, Geirsson A, Sumpio BE, Moll FL, Muhs BE. Endograft collapse after thoracic endovascular aortic repair. J Endovasc Ther. 2010;17:725-34.

[13] Muhs BE, Balm R, White GH, Verhagen HJM. Anatomic factors associated with acute endograft collapse after Gore TAG treatment of thoracic aortic dissection or traumatic rupture. Journal of Vascular Surgery. 2007;45:655-61.

[14] Shukla AJ, Jeyabalan G, Cho JS. Late collapse of a thoracic endoprosthesis. Journal of Vascular Surgery. 2011;53:798-801.

[15] Pasta S, Cho JS, Dur O, Pekkan K, Vorp DA. Computer modeling for the prediction of thoracic aortic stent graft collapse. Journal of Vascular Surgery. 2013;57:1353-61.

[16] Tsai TT, Schlicht MS, Khanafer K, Bull JL, Valassis DT, Williams DM, et al. Tear size and location impacts false lumen pressure in an ex vivo model of chronic type B aortic dissection. J Vasc Surg. 2008;47:844-51.

[17] Pasta S, Rinaudo A, Luca A, Pilato M, Scardulla C, Gleason TG, et al. Difference in hemodynamic and wall stress of ascending thoracic aortic aneurysms with bicuspid and tricuspid aortic valve. J Biomech. 2013;46:1729-38.

[18] D'Ancona G, Lee JJ, Pasta S, Pilato G, Rinaudo A, Follis F, et al. Computational analysis to predict false-lumen perfusion and outcome of type B aortic dissection. J Thorac Cardiovasc Surg. 2014;148:1756-8.

[19] Morris L, Delassus P, Walsh M, McGloughlin T. A mathematical model to predict the in vivo pulsatile drag forces acting on bifurcated stent grafts used in endovascular treatment of abdominal aortic aneurysms (AAA). J Biomech. 2004;37:1087-95.

[20] Dur O, DeGroff CG, Keller BB, Pekkan K. Optimization of Inflow Waveform Phase-Difference for Minimized Total Cavopulmonary Power Loss. Journal of Biomechanical Engineering-Transactions of the Asme. 2010;132:-.

[21] Raghavan ML, Vorp DA. Toward a biomechanical tool to evaluate rupture potential of abdominal aortic aneurysm: identification of a finite strain constitutive model and evaluation of its applicability. Journal of Biomechanics. 2000;33:475-82.

[22] Lam SK, Fung GS, Cheng SW, Chow KW. A computational study on the biomechanical factors related to stent-graft models in the thoracic aorta. Med Biol Eng Comput. 2008;46:1129-38.

[23] van Bogerijen GH, Auricchio F, Conti M, Lefieux A, Reali A, Veneziani A, et al. Aortic hemodynamics after thoracic endovascular aortic repair, with particular attention to the bird-beak configuration. J Endovasc Ther. 2014;21:791-802.

[24] Cheng SW, Lam ES, Fung GS, Ho P, Ting AC, Chow KW. A computational fluid dynamic study of stent graft remodeling after endovascular repair of thoracic aortic dissections. J Vasc Surg. 2008;48:303-9; discusion 9-10.

[25] Fung GS, Lam SK, Cheng SW, Chow KW. On stent-graft models in thoracic aortic endovascular repair: a computational investigation of the hemodynamic factors. Computers in biology and medicine. 2008;38:484-9.

[26] Auricchio F, Conti M, Marconi S, Reali A, Tolenaar JL, Trimarchi S. Patient-specific aortic endografting simulation: from diagnosis to prediction. Computers in biology and medicine. 2013;43:386-94.

[27] Auricchio F, Conti M, Lefieux A, Morganti S, Reali A, Sardanelli F, et al. Patient-specific analysis of post-operative aortic hemodynamics: a focus on thoracic endovascular repair (TEVAR). Comput Mech. 2014;54:943-53.

[28] Pelton AR, Schroeder V, Mitchell MR, Gong XY, Barney M, Robertson SW. Fatigue and durability of Nitinol stents. Journal of the mechanical behavior of biomedical materials. 2008;1:153-64.

[29] Leung DA, Davis I, Katlaps G, Tisnado J, Sydnor MK, Komorowski DJ, et al. Treatment of infolding related to the gore TAG thoracic endoprosthesis. Journal of vascular and interventional radiology : JVIR. 2008;19:600-5.

[30] Farber MA, Giglia JS, Starnes BW, Stevens SL, Holleman J, Chaer R, et al. Evaluation of the redesigned conformable GORE TAG thoracic endoprosthesis for traumatic aortic transection. J Vasc Surg. 2013;58:651-8.

[31] Rudenick PA, Bijnens BH, Garcia-Dorado D, Evangelista A. An in vitro phantom study on the influence of tear size and configuration on the hemodynamics of the lumina in chronic type B aortic dissections. J Vasc Surg. 2013;57:464-74 e5.

Figure Legends

Figure 1: (A) Schematic of pulsatile flow circuit; (B) photography of phantom model with particulars of bird-beak configurations with PE=19 mm; (C) pressure profiles measured for bird-beak configuration with PE=19 mm and θ =20 deg at different cardiac outputs; (D) flow profiles measured at aortic inlet. The accuracy of infolding measurement was 29 μm for a field of view of 30 x 35 mm with images acquired at 30 fps.

Figure 2: TAG compliance profiles obtained after interative (manual) calibration of infolding parameters for the investigated hemodynamic scenarios (R^2>0.96 for all fitting curves)

Figure 3: Pressure distribution (row above) and velocity streamlines (row below) at systolic peak for all patients with a protruded endograft wall; Case A with PE=19mm; Case B with PE=21mm; Case C with PE=26mm; Case D with PE=28mm

Figure 4: Distributions of Mises's stress (row above) and strain (row below) of the protruded endograft walls estimated at peak of systole; Case A with PE=19mm; Case B with PE=21mm; Case C with PE=26mm; Case D with PE=28mm

Table 1: TAG device displacements experimentally measured under different perfusion conditions.

	TAG Device Displacement (mm)		
	ΔP=90/55mmHg; CO=3L/min	ΔP=120/80mmHg; CO=5L/min	ΔP=170/100mmHg; CO=7L/min
PE=13mm	0.26	0.39	0.65
PE=19mm	0.60	0.89	1.20
PE=24mm	0.72	1.01	1.66

Note: DP: systemic pressure; CO: cardiac output

Table 2: Transmural pressure across the protruded endograft wall and endograft displacements for all patients; Case A with PE=19mm; Case B with PE=21mm; Case C with PE=26mm; Case D with PE=28mm

	Case A	Case B	Case C	Case D
Transmural Pressure (mmHg)	0.89	1.26	2.85	8.72
Endograft Displacement (mm)	0.89	1.18	4.10	3.15

Fig 1

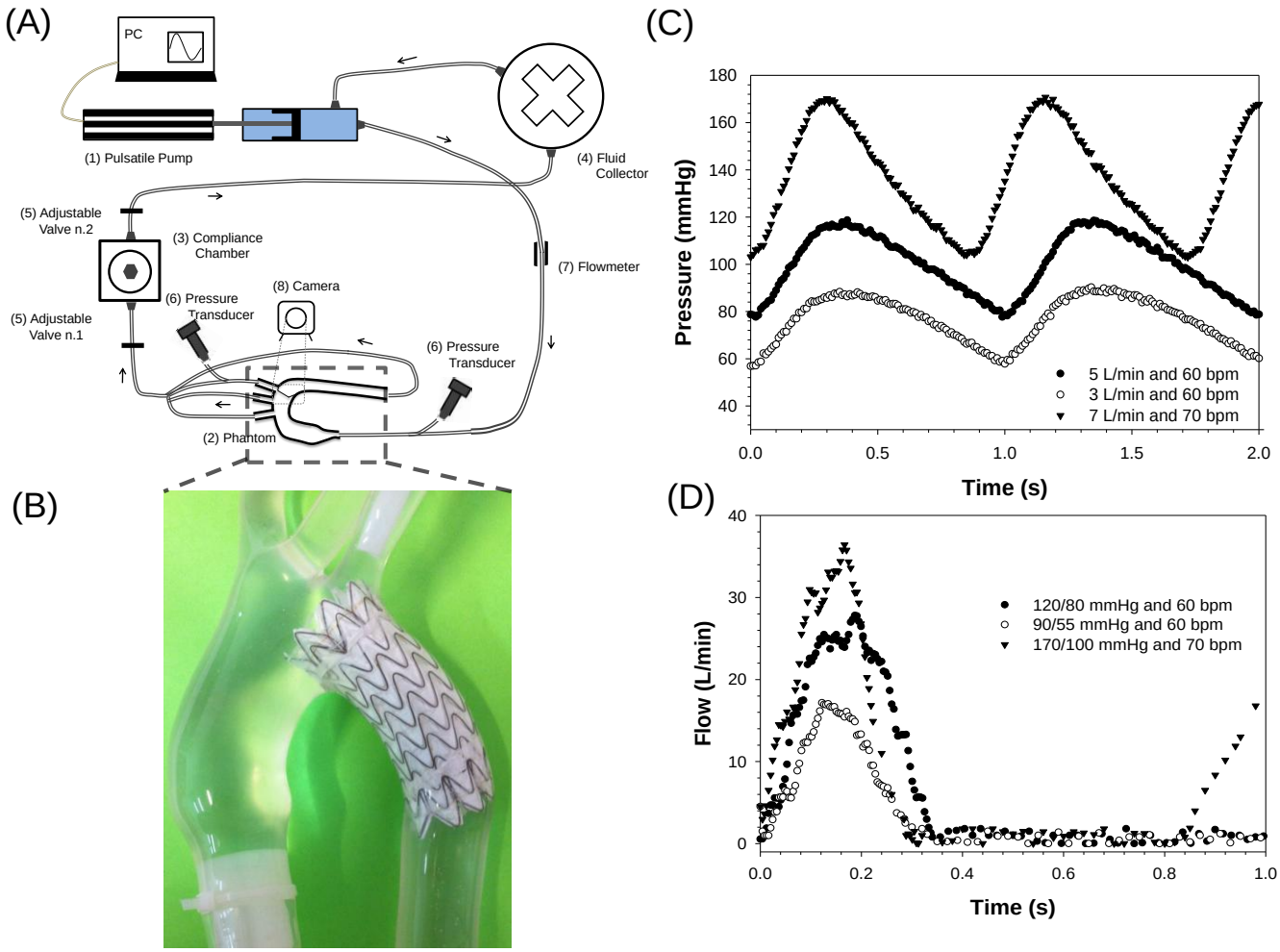
(A)
PC
(1) Pulsatile Pump
(4) Fluid Collector
(5) Adjustable Valve n.2
(3) Compliance Chamber
(7) Flowmeter
(6) Pressure Transducer
(8) Camera
(5) Adjustable Valve n.1
(6) Pressure Transducer
(2) Phantom
(B)
(C)
Pressure (mmHg)
Time (s)
5 L/min and 60 bpm
3 L/min and 60 bpm
7 L/min and 70 bpm
(D)
Flow (L/min)
Time (s)
120/80 mmHg and 60 bpm
90/55 mmHg and 60 bpm
170/100 mmHg and 70 bpm

Fig 2

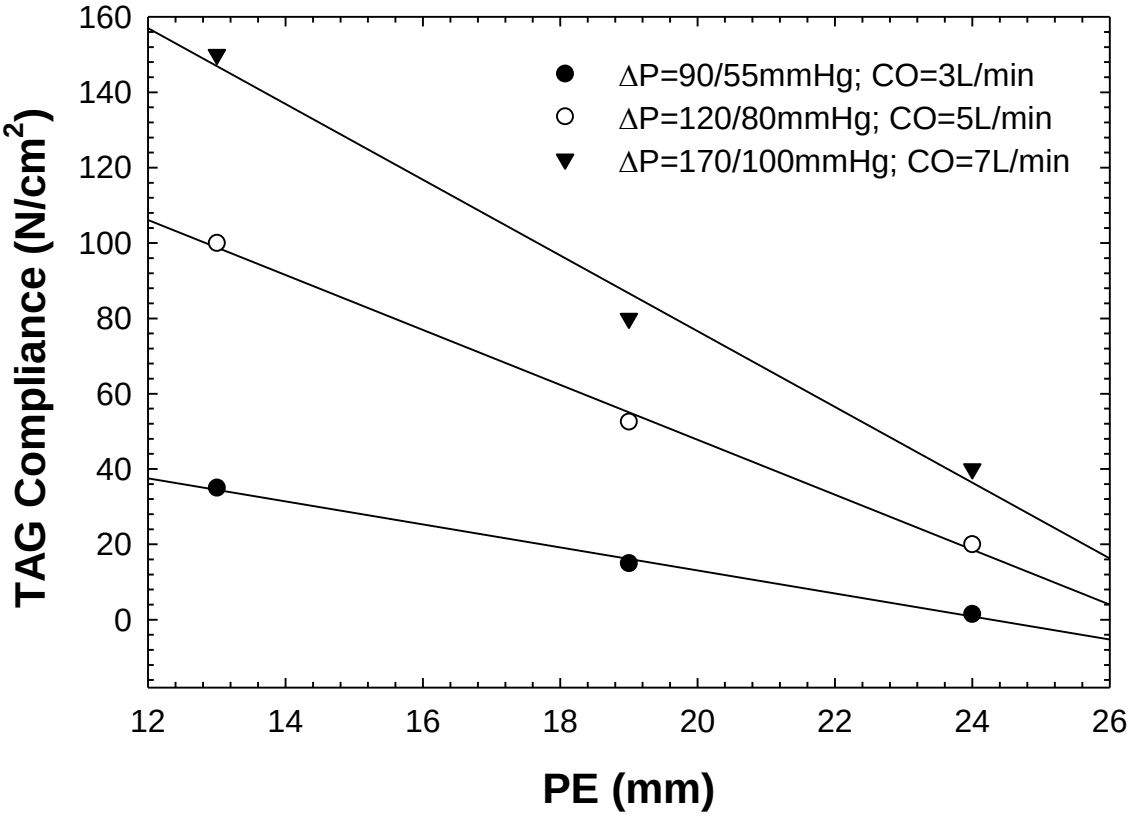
TAG Compliance (N/cm2)
PE (mm)
ΔP=90/55mmHg; CO=3L/min
ΔP=120/80mmHg; CO=5L/min
ΔP=170/100mmHg; CO=7L/min
160
140
120
100
80
60
40
20
0
12
14
16
18
20
22
24
26

Fig 3

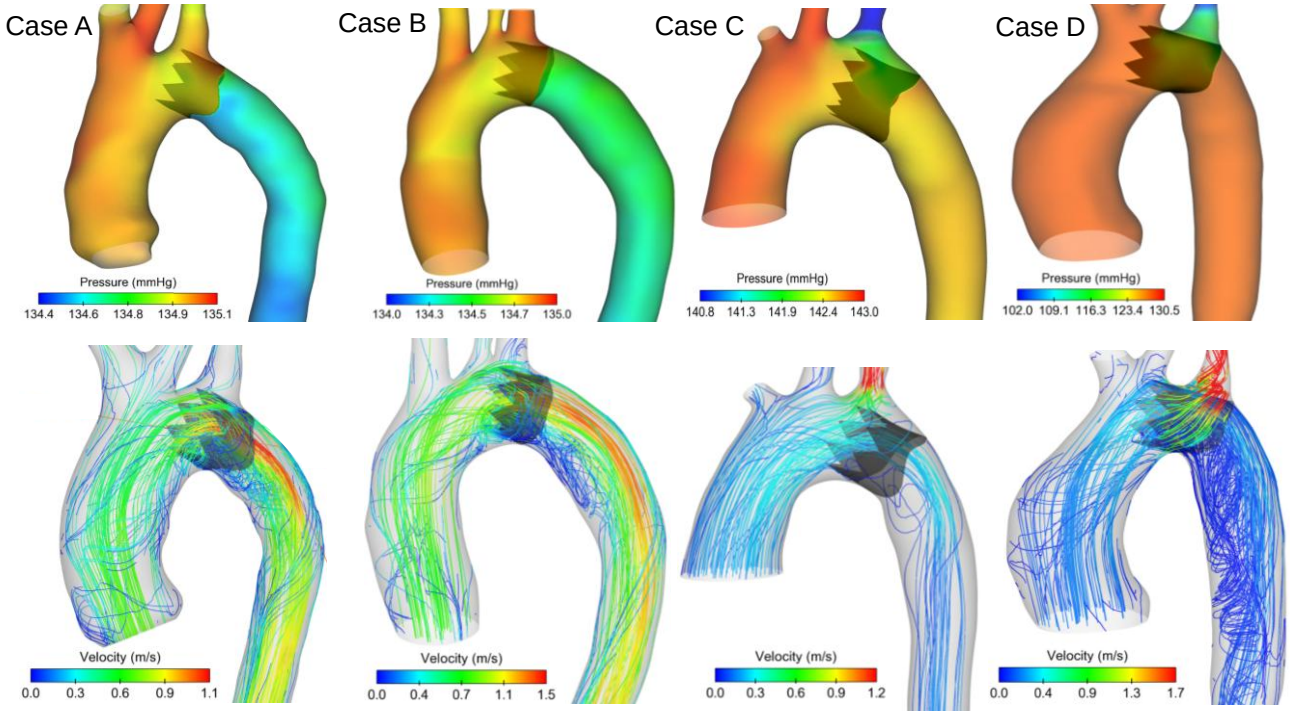
Case A
Case B
Case C
Case D
Pressure (mmHg)
134.4 134.6 134.8 134.9 135.1
Pressure (mmHg)
134.0 134.3 134.5 134.7 135.0
Pressure (mmHg)
140.8 141.3 141.9 142.4 143.0
Pressure (mmHg)
102.0 109.1 116.3 123.4 130.5
Velocity (m/s)
0.0 0.3 0.6 0.9 1.1
Velocity (m/s)
0.0 0.4 0.7 1.1 1.5
Velocity (m/s)
0.0 0.3 0.6 0.9 1.2
Velocity (m/s)
0.0 0.4 0.9 1.3 1.7

Fig 4

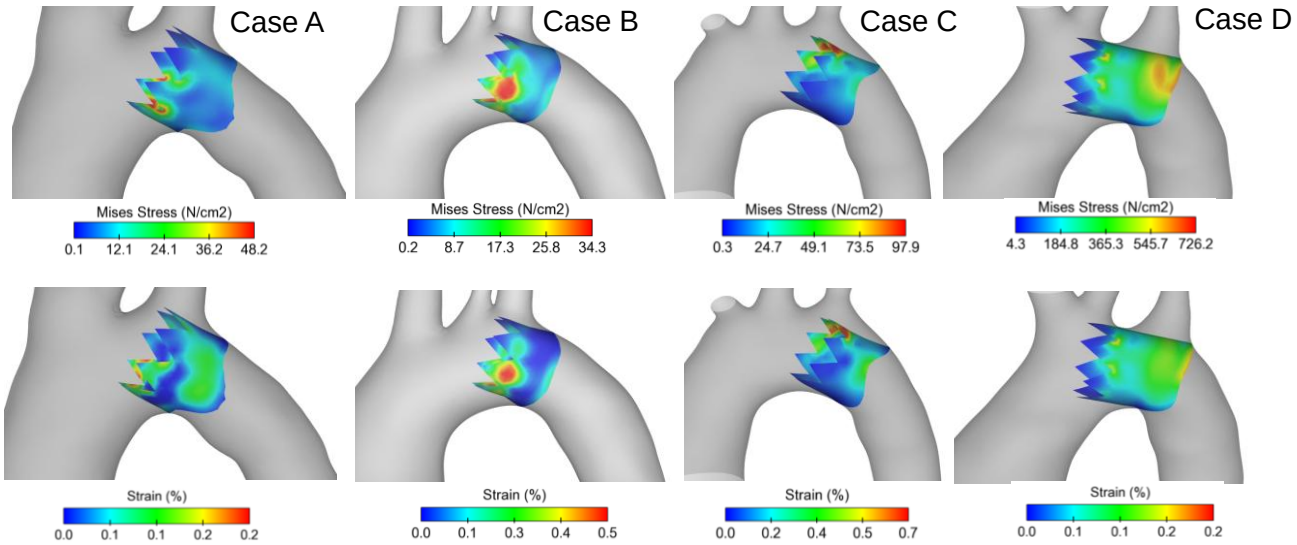
Case A
Case B
Case C
Case D
Mises Stress (N/cm2)
0.1 12.1 24.1 36.2 48.2
Mises Stress (N/cm2)
0.2 8.7 17.3 25.8 34.3
Mises Stress (N/cm2)
0.3 24.7 49.1 73.5 97.9
Mises Stress (N/cm2)
4.3 184.8 365.3 545.7 726.2
Strain (%)
0.0 0.1 0.1 0.2 0.2
Strain (%)
0.0 0.1 0.3 0.4 0.5
Strain (%)
0.0 0.2 0.4 0.5 0.7
Strain (%)
0.0 0.1 0.1 0.2 0.2